Design and Analysis of Solar-Powered Automatic Thermoelectric Cooling System for Automobile Cabin

Alemnew Achaye Admassie

A Thesis Submitted to

The Department of Mechanical Systems and Vehicle Engineering

School of Mechanical, Chemical and Materials Engineering

Presented in Partial Fulfillment of the Requirement for the Degree of Masters of Science in Automotive Engineering

Office of the Graduate Studies

Adama Science and Technology University

October 2021

Adama, Ethiopia

Design and Analysis of Solar-Powered Automatic Thermoelectric Cooling System for Automobile Cabin

Alemnew Achaye Admassie

Advisor: Ramesh Babu Nallamothu (Ph.D)

A Thesis Submitted to

The Department of Mechanical Systems and Vehicle Engineering

School of Mechanical, Chemical and Materials Engineering

Presented in Partial Fulfillment of the Requirement for the Degree of Masters of Science in Automotive Engineering

Office of Graduate Studies

Adama Science and Technology University

October 2021

Adama, Ethiopia

DECLARATION

I hereby declare that this Master Thesis entitled "Design and Analysis of Solar-Powered Automatic Thermoelectric Cooling System for Automobile Cabin" is my original work. That is, it has not been submitted for the award of any academic degree, diploma or certificate in any other university. All sources of materials that are used for this thesis have been duly acknowledged through citation.

Name of the student	Signature	Date

RECOMMENDATION

We, the advisor(s) of this thesis, hereby certify that we have read the revised version of the thesis entitled “Design and Analysis of Solar-Powered Automatic Thermoelectric Cooling System for Automobile Cabin” prepared under my/our guidance by Alemnew Achaye submitted in partial fulfillment of the requirements for the degree of Master of Science in Automotive Engineering. Therefore, we recommend the submission of revised version of the thesis to the department following the applicable procedures.

____________________	____________________	______________
Advisor name	Signature	Date
____________________	____________________	______________
Co-advisor name	Signature	Date

APPROVAL PAGE

I/we, the advisors of the thesis entitled "Design and Analysis of Solar-Powered Automatic Thermoelectric Cooling System for Automobile Cabin" and developed by Alemnew Achaye hereby certify that the recommendation and suggestions made by the board of examiners are appropriately incorporated into the final version of the thesis.

____________________	____________	____________
Major Advisor	Signature	Date
____________________	____________	____________
Co-advisor	Signature	Date

We, the undersigned, members of the Board of Examiners of the thesis by Alemnew Achaye have read and evaluated the thesis entitled "Design and Analysis of Solar-Powered Automatic Thermoelectric Cooling System for Automobile Cabin" and examined the candidate during the open defense. This is, therefore, to certify that the thesis is accepted for partial fulfillment of the requirement of the degree of Master of Science in Automotive Engineering.

____________________	____________	____________
Chairperson	Signature	Date
____________________	____________	____________
Internal Examiner	Signature	Date
____________________	____________	____________
External Examiner	Signature	Date

Finally, approval and acceptance of the thesis is contingent upon submission of its final copy to the Office of Postgraduate Studies (OPGS) through the Department Graduate Council (DGC) and School Graduate Committee (SGC).

____________________	____________	____________
Department Head	Signature	Date
____________________	____________	____________
School Dean	Signature	Date
____________________	____________	____________
Office of Postgraduate Studies, Dean	Signature	Date

ACKNOWLEDGMENT

First and foremost, my deepest gratitude goes to the almighty God for being with me in every aspects of my life and for giving me the strength to do this thesis. I would like to thank my advisor Dr. Ramesh Babu Nallamothu for his continuous encouragement and constructive comments from the beginning of this work up to the final. He has been guiding me and teaching me valuable lessons.

I would like to express my sincere gratitude to my family and everyone who helped me finish this thesis and finally I would like to thank Adama Science and Technology University for giving me the chance to join the master’s program with full sponsorship.

ABSTRACT

The cabin temperature of a closed stationary vehicle in direct sunlight can quickly rise to a level that may damage property and harm children or pets left in the vehicle. The problem that is faced by many car users today is a hot interior after certain minutes or hours of parking in un-shaded parking areas. A primary goal of cabin thermal management design is to minimize vehicle energy use while achieving a high level of passenger comfort. Vehicle heating, ventilation, and air-conditioning (HVAC) systems exert a large power demand on the vehicle's engine and battery, which can lead to reduced fuel economy. But, when the car is parked it is not economical to use the system provided by the manufacturers to start the air conditioner as it requires the engine to remain "ON" to match the power required. This is not economical at all. Thus, the idea of using the car's inbuilt air conditioner to cool the car while it's parked is dropped, and decided to build a new cooling system to cool the cabin and be economical at the same time which runs on solar power. In addition, for a parked car, the cooling system should be automatic as there is no one to detect the heat and run the cooling system. This problem is solved by designing a solar-powered automatic thermoelectric cooling system for automobile cabins. The heat gain by the car cabin parked in direct sunlight is analytically estimated. Heat sinks and thermoelectric modules are designed. For the optimization of the design of the thermoelectric module and the heat sinks, Mathcad software has been used. The aerodynamic effect of the cooling system for the car has also been assessed using ANSYS FLUENT 19.3. A demo is made with a 1:8 reduction scale from aluminum sheet metal of thickness 0.8 mm as the body material. Carton having a thickness of 0.2 mm has been used as an insulating material from inside. For demonstration, the TEC1-12706 module, CPU cooling fans, and aluminum heat sinks are also used. From the design, the TEC module whose optimum cooling capacity is 37.8 W obtained. Eight TEC modules each with two heat sinks and cooling fans are used for the cooling system. The total cooling capacity of the thermoelectric cooling system is 267.24 W. In general, the cooling system can have a significant role in reducing the rate of temperature rise of cabin air. The increase in the aerodynamic drag coefficient due to the assembly of the thermoelectric cooling system to the car is 0.73%. From the demonstration of the thermoelectric cooling system, the cabin air temperature of the model is found to be lower by more than 3 ℃ when the cooling system was running.

Keywords: Thermoelectric, Seebeck effect, Peltier effect, TEC module, Cooling system

TABLE OF CONTENTS

CONTENTS **PAGE**

LIST OF TABLES

TABLES **PAGE**

LIST OF FIGURES

FIGURE **PAGE**

LIST OF ACRONYMS

AAC	Automotive Air Conditioning
ASHRAE	American Society of Heating, Refrigeration and Air Conditioning Engineers
COP	Coefficient of Performance of TEC
HVAC	Heating, Ventilation, and Air Conditioning
TEC	Thermoelectric Cooler
TEG	Thermoelectric Generator
ZT	Thermoelectric dimensionless figure of merit

NOMENCLATURE

A	Area (m^2)
A_c	Cross flow area of the heat sink
B	Height of fins of a heat sink *(mm)*
C	Specific heat *(J/kgK)*
H	Convection heat transfer coefficient (W/m^2K)
I	Hourly incident solar radiation (W/m^2)
I_{maxp}	Maximum current for the maximum cooling power *(A)*
I_{opt}	Optimum current *(A)*
k	Thermal conductivity of a material *(W/mK)*
K	Thermal conductance (*W/K*)
k'	Heat capacity per unit area (J/m^2k)
L	Length (m)
M	Passenger metabolic heat production rate (W/m^2)
m	Mass (kg)
n	Number of thermocouples
N	Number of thermo-elements
Q	The rate of heat transfer *(W)*
R	Thermal resistance (m^2K/W)

Re	Electrical resistance (ohm)
T	Temperature (K)
t	Time (S)
U	Overall heat transfer coefficient (W/m^2K)
V	Speed (m/s)
V_{fr}	Volume flow rate *(cfm)*
W	Electrical power (W)
x	The thickness of the surface element *(mm)*
Z	The figure of merit of a thermoelectric material (K^{-1})
Z_{opt}	Optimum fin spacing for heat sinks *(mm)*
Z_θ	Zenith angle (°)
ρ_g	Ground reflectivity coefficient

GREEK SYMBOLS

α	Seebeck coefficient of a thermoelectric material (V/K)
β	The altitude angle that is calculated based on position and time (°)
γ	Surface azimuth angle (°)
θ	The angle of incidence (°)
ε	Slope or tilt angle of a surface from the horizontal (°)
τ	Surface element transmissivity
φ	Latitude angle (°)
ω	The hour angle of the sun east or west of the local meridian (°)
δ	Declination angle of the sun at solar noon with respect to the plane of the equator (°)
ρ	Electrical resistivity of a material (Ωcm)
Γ	Thomson coefficient of a thermoelectric material
Π	Peltier coefficient of a material (W/AK)
η	Efficiency
Δ	Change/gradient

SUBSCRIPTS

a	Air	*h*	Hot side
amb	Ambient	*h,a*	Hot side to ambient
c	Cold side	*i*	Inside /internal
comf	Comfortable	*j,c*	Junction to cold side
Dir	Direct	*n*	N-type element
Diff	Diffuse	*m*	Module
Du	Dubois	*o*	Outside/external
Eng	Engine	*opt*	Optimum
Exh	Exhaust	*p*	P-type element
f	Fin	*Ref*	Reflected
fr	Flow rate	*s*	Surface element

CHAPTER ONE

INTRODUCTION

1.1. Background of the Study

Nowadays the number of vehicles in the world is drastically increasing. So many people use these vehicles for transportation purposes.

The cabin temperature of closed stationary vehicles in direct sunlight can quickly rise to a level that may damage property and harm children or pets left in the vehicle. The problem that is faced by many car users today is a hot interior after certain minutes or hours of parking in un-shaded parking areas. The accumulation of thermal energy inside the vehicle with undesired temperature rise would cause the interior parts to degrade because they normally are subjected to wear and tear. Degradation may shorten the life span of the various components inside the car. Passengers are also affected by the thermal condition inside the vehicle itself. The car user is forced to wait for some time before getting into the car to cool down the interior condition by either rolling down the window or running the air conditioner at a high speed that affects the fuel consumption (M. Purusothaman *et al.*, 2017).

Reducing heat accumulation within vehicles and ensuring appropriate vehicular temperature levels can lead to enhanced vehicle fuel economy, range, reliability, passenger comfort, and safety. Advancements in vehicle thermal management remain key as new technologies; consumer demand, societal concerns, and government regulations emerge and evolve.

Car Cabin

The cabin consists of structural components that separate the internal, temperature-controlled environment from the external environment of a vehicle. In this regard, the cabin area serves as a main focal point in ensuring the overall comfort of the passenger, by not only providing an environment that allows for a pleasant driving experience but also ensuring that the thermal conditions within the cabin are conducive to alert driving habits. Danca *et al.* (2016) discuss the measurement and improvement of passenger comfort in detail.

A primary goal of cabin thermal management design is to minimize vehicle energy use while achieving a high level of passenger comfort. Vehicle heating, ventilation, and air-conditioning (HVAC) systems exert a large power demand on the vehicle's engine and battery, which can lead to reduced fuel economy. A study involving a group of vehicles with different sizes and HVAC systems, and an average fuel economy of 41 US miles per gallon (MPG; 1 MPG $\approx$ 2.35 L·km^{-1}), demonstrated that fuel consumption increased by 23%–41% when the air conditioner (AC) was operating. Being able to reduce fuel consumption not only decreases gasoline/diesel costs for the vehicle owner but also has a positive impact on the environment by reducing harmful emissions (Bjurling, 2013; Marshall *et al*., 2019).

1.2. Statement of the Problem

Whenever a car is parked under direct sunlight, the inside temperature can rise to dangerously threatening levels. According to the data recorded for the cabin air temperatures at solar noon, it could reach more than 46℃ (see Table C.1). The sunlight is absorbed by the surface of the car (e.g., dashboard and the carpet). Since sunlight is radiated energy, the impact surface heats up due to the absorption of this radiated energy. Sunlight falls on the carpet and plastic parts within the car and then they re-radiate that energy in the infrared spectrum. Now, water vapor and CO in the air within the car absorb this re-radiated IR energy, and thus, the heat is accumulated continuously. This heat is trapped inside the car, as there is no exit point. To reduce this heat accumulation in the car cabin, an A/C system must run. But, when the car is parked it is not recommended to start the air conditioner as it requires the engine to remain "ON". This is not economical at all. Thus, the idea of using the car's inbuilt air conditioner to cool the car while it's parked is dropped, and decided to build a new cooling system to cool the cabin and be economical at the same time which runs on solar power. In addition to this, since, the conventional A/C system is manually operated it could not automatically be started for a parked vehicle as there is no one inside to detect the heat and run the system. The above reasons constitute a good motivation for the design of a solar-powered automatic thermoelectric cooling system.

1.3. Objectives

1.3.1. General objective

The general objective of this thesis is to design a solar-powered automatic thermoelectric cooling for automobiles cabin to increase car cabin thermal comfort during parking.

1.3.2. Specific objectives

The specific objectives of this thesis are:

- ✓ To estimate the cooling load of the car cabin
- ✓ To design the thermoelectric cooler module and the heat sinks for the cooling system
- ✓ To analyze the cooling performance of the designed thermoelectric cooling system
- ✓ To demonstrate the use of the thermoelectric cooling system for the vehicle during parking
- ✓ To assess the aerodynamic effect of the cooling system using ANSYS FLUENT software.

1.4. Significance of the Study

This study helps to reduce the cabin temperature of a parked vehicle so that the driver or passenger will not feel uncomfortable when he gets back to his car, parked in a direct sunlight region. The cooling system minimizes this discomfort. Additionally, vehicle body parts (seat, dashboard) and objects placed in the vehicle will not degrade due to the thermal energy, which could have been accumulated in the cabin. It also increases fuel economy which should have been used for running an AC to minimize cabin temperature. The beneficiaries of this study are car owners, organizations, a state, and at large the world.

1.5. Scope of the Thesis Work

In this paper, an automatic solar-powered thermoelectric cooling system is designed. Although it is possible to design the system for other vehicles, due to the available time and resources, this work mainly focuses on small cars/automobiles particularly the Toyota Vitz 2008 model. Cooling load estimation and design of heat sinks have been conducted. How the thermoelectric cooling system works is demonstrated. Finally, the aerodynamic effect of the cooler assembly, which is installed on the roof of the car, is also assessed using ANSYS FLUENT 19 R3 software.

1.6. Limitations of the Study

Some factors limited this thesis work. The availability of the components is the main limiting factor. For demonstration, aluminum heat sink and cooling fans of the required dimension are not found.

1.7. Organization of the Study

This paper is organized into the following chapters;

Chapter 1: Introduction: - In this part, what the study focuses on and the introduction to the study area have been presented. Statement of the problem, objective, and scope of the thesis is explained in this chapter.

Chapter 2: Literature reviews: Literature related to the study area (air conditioning, thermoelectricity, etc.) has been reviewed and presented. Previous works on the title and research gaps are mentioned.

Chapter 3: Materials and methodology: - Under this chapter, the materials, which have been used to conduct this paper and the methodology followed, are explained. In this section, theoretical analysis and design of the cooling system have been conducted. The heat gain by the cabin from various heat sources is estimated. The system component sizing and selection is performed in this chapter. The thermoelectric cooling system is practically demonstrated in this chapter.

Chapter 4: Result and discussion: - In this chapter: the design result of the heat sinks, TEC module, and aerodynamic assessment results are discussed. The performance evaluation of the automatic thermoelectric cooling system is held under this section.

Chapter 5: Conclusion and Recommendation: - In this section, the conclusions are drawn from the study and future recommendations in the area are listed.

CHAPTER TWO

LITERATURE REVIEW

In this chapter, different pieces of literature related to this study have been reviewed and presented. Journals, books, websites, and different published papers are used to review what is related to this Thesis. Literature that focused on thermoelectricity is well-reviewed. Previous works which are conducted by researchers are also reviewed. Finally, a literature summary and research gaps in this area are put.

2.1. Automotive Conventional Air Conditioning

Automotive air conditioning is the process by which the air inside the car cabin is cooled and cleaned, the humidity lowered, and the air circulated. The quantity and quality of the air are also controlled. Under ideal conditions, the air-conditioning system can be expected to accomplish all these tasks at the same time (Agarwal & Khan, 2018).

Components of the air conditioning system are compressors, condensers, filter dryer, expansion valve, evaporator, pressure switch, ventilation fan, and condenser fan.

Limitations of conventional HVAC system

In a modern automobile, the A/C system will use around four horsepower (3 kW) of the engine's power, thus increasing the fuel consumption of the vehicle (Agarwal & Khan, 2018). Combustion of one liter of petrol also emits 240 gm of carbon monoxide, 2.5 gm of carbon Dioxide, 1 gm of hydrocarbons, and 0.1 gm of nitrogen oxide (Lethwala & Garg, 2017). The emissions of these pollutant gases lead to global warming so it is a very serious case to the world. Due to the above problem and other reasons, other alternatives to car cooling systems are being experimented with.

Below is a summary of the drawback of the conventional air conditioning system *(*Pache *et al*., 2014);

Power loss: the crankshaft of the engine drives the Compressor. That means the A/C compressor consumes 5 to 10% of engine power.

Fuel loss: Present HVAC System reduces the mileage of the vehicle.

Electric loss: Battery provides 12V current to the blowers and electromagnetic clutch of compressor for engaging the compressor.

Cost: The cost of the present HVAC System is very high.

Hazardous refrigerant: Hydrofluorocarbons are quite hazardous for the human body & the ozone layer, which leads to global warming.

Repairing cost: The repairing cost of the HVAC System is very high.

Maintenance: Proper maintenance is very necessary because this system can affect the human body & Environment.

Size: Present HVAC system required a very large space in the engine compartment and dashboard.

Delicate system: If any component fails to perform well then, the whole HVAC system will either not function properly or not function at all.

It can't run without the engine. It is dependent on engine operation/state.

2.2. An Alternative Approach for Car Cabin Comfort

The remarkable outcomes of the experiment on car cabin comfort resulted in many design reconsiderations by the automobile manufacturers, but it still left us unanswered with a major challenge, i.e., cooling, the greenhouse effect, and harmful emission inside the car cabin. The most promising method to handle the challenge of the greenhouse effect, harmful emission inside the car cabin, and to cool the car cabin is to provide for a system of air conditioning and ventilation in the car. It is not the conventional system provided along by the manufacturer, but rather an alternate system that works without consuming the fuel or running the engine while the car is parked in the sun (Singh, 2015).

Lethwala & Garg, (2017) discussed a feasibility study of an existing air conditioner using solar energy. With the implementation of solar conditioners in an automobile, fuel efficiency will be increased and tailpipe emissions are reduced. Also, by detaching, a compressor from the engine and making it run through the solar energy, the load on the engine decreases. The air conditioner compressor can be run with the help of 230 V, A/C motor of power 738 watts. They estimated that if a 100 W power solar panel is installed on the roof of the car with a maximum solar power point tracking device, then the power produced from the solar panel per day could run the car A/C for 1 hour a day at peak load.

The challenge for this system is that the maximum solar power point tracker, which is to be installed on the roof of the car, increases the aerodynamic drag decreases the stability of the vehicle. The other challenge is that the power obtained from solar power is seasonal. As a result, constant power cannot be obtained for running the system. This study could not be feasible due to the listed drawbacks.

2.2.1. Thermoelectric cooling

The thermoelectric effect can be defined as the direct conversion of temperature difference to electric voltage and vice versa. The thermoelectric effect covers three different identified effects namely, the Seebeck effect, Peltier effect, and the Thomson effect. A thermoelectric device will create a voltage when there is a temperature difference on each side of the device On the other hand when a voltage is applied to it, a temperature difference is created (Patil, 2014).

2.2.1.1. Discovery of Peltier effect and its use in cooling

Jean Peltier discovered in 1834 that "with the two junctions of a thermocouple at the same temperature if an electric current is passed through the thermocouple, heat is evolved at one junction and absorbed at the other junction". Although this effect was discovered in 1834, there was no idea to use this phenomenon for refrigerators or air conditioners as the electricity itself was not yet used as 'energy' at the time. Michael Faraday had discovered the law of practical electric generation or electrical induction in 1831. It took over 50 years from this discovery to the commercialization of alternate current electricity generators. It was in 1954 that people had ideas to make thermoelectric refrigerators or air conditioners i.e., about 70 years later from the first commercial alternate current generation. In this year, N.E. Lindenblad, American, made a small refrigerator using lead/telluride (PbTe) and antimony/telluride (SbTe) as the thermoelectric junctions. In the same year, H.J. Goldsmid, at General Electric Company, got a remarkable ΔT of 26°C, never obtained before, using Bi_2Te_3/Sb_2Te_3 as the P-type and Bi as the N-type. In the next year, 1955, his group obtained an outstanding ΔT of 46°C with the thermoelectric junction of P and N-type bismuth telluride. The rapid performance enhancement of bismuth telluride made this material a promising choice with far better performance. For this reason, experimental fabrication of refrigerators and air conditioners, targeting future use of them in offices and homes, was done (Abdul & Uit, 2017).

1. Seebeck Effect

In 1821, Seebeck observed that if two different or dissimilar materials are joined and the junctions between them are held at different temperatures (T and $T + \Delta T$), then a voltage difference (ΔV) is developed. This voltage is found to be proportional to the temperature difference (ΔT); see Figure 2.1. This phenomenon is called the Seebeck effect. The ratio of the voltage generated to the temperature gradient is an intrinsic property of the material, and it is called the Seebeck coefficient, α, where $\alpha = -\Delta V / \Delta T$ (Goldsmid, 2016). The temperature difference results in moving the mobile charge carriers (electrons or holes) towards the cold junction and leaving behind the oppositely charged and immobile nuclei at the hot junction. Charge movement results in the rise of a thermoelectric voltage.

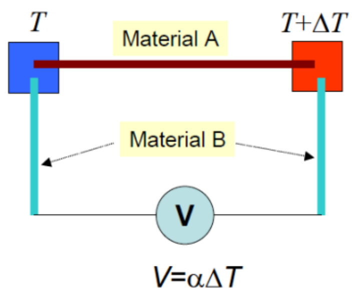

Figure 2.1: Seebeck effect.
(https://www.sciencedirect.com/topics/chemistry/thermoelectric-effect)

The thermoelectric voltage (V) generated is given by (Goldsmid, 2016);

$$V = (\alpha_A - \alpha_B)\Delta T \tag{2.1}$$

Where, α_A and α_B are the Seebeck coefficients of the materials A and B, respectively, and ΔT is the temperature difference between the junctions.

2. **Peltier Effect**

The Peltier effect is another important principle of the thermoelectric phenomenon. This effect explains that if an electrical current flows through the junction of two dissimilar materials, it will generate or absorb heat depending on the direction of the current. The reason for this is the same as the Seebeck effect. The applied current causes electrons to flow through the thermoelectric. In doing so, the electrons carry thermal energy from one side to the other (Nair & Tripathi, 2019).

The Peltier heat, (Q), absorbed or rejected by the junction is given by (Willfahrt, 2014; Franklin, 2018);

$$dQ/dT = I(\Pi_A - \Pi_B) \tag{2.2}$$

Where Π_A and Π_B are the Peltier coefficient of materials A and B, respectively, and I, is the current passed through the materials. The Peltier coefficient represents the amount of heat absorbed by the material when current passed through it.

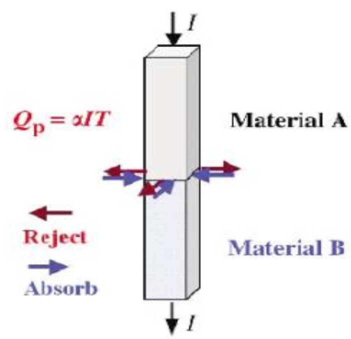

Figure 2.2: Peltier effect (Tritt, 2002).

The Thomson effect occurs when there is a temperature gradient across a conductor accompanied by a current. Heat can either be released or absorbed depending on the flow of current and the temperature gradient. The amount of heat absorbed or released (Goldsmid, 2016) is:

$$Q_{Thomson} = \Gamma I \Delta T \tag{2.3}$$

Where, Γ is the Thomson coefficient and is given as (Goldsmid, 2016);

$$\Gamma = T\frac{d\alpha}{dT} \tag{2.4}$$

The Thomson effect is the only thermoelectric effect, which can be experienced by a single conductor. The Seebeck and Peltier effects require two conductors to be connected at a junction

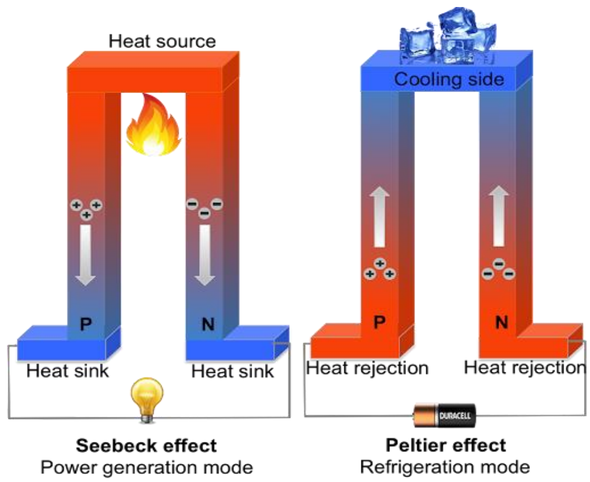

Figure 2.3: Seebeck and Peltier effect for N-type and P-type material

[http://howthingswork.org/physics-thermoelectric-effect-physics-and-applications/2/]

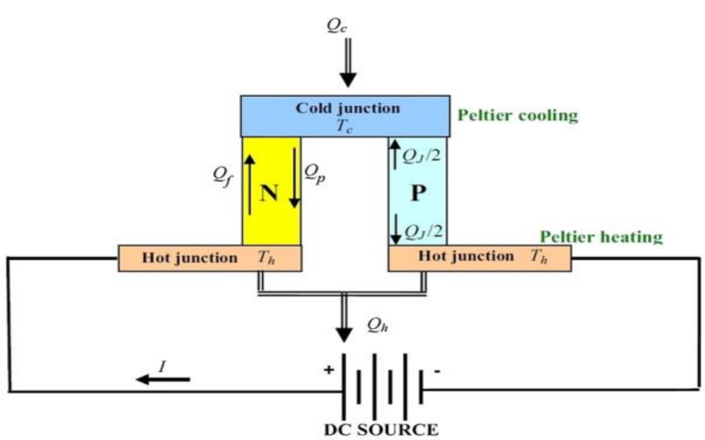

Figure 2.4: Schematic of a thermoelectric module (Sarbu & Dorca, 2018).

The above figure 2.4 illustrates a TEC cooling module considered as a TEC refrigerator, in which the electrical current flows from the N-type element to the P-type element. The temperature T_c of the cold junction decreases and the heat is transferred from the environment to the cold junction at a lower temperature. This process happens when the transport electrons pass from a low-energy level inside the P-type element to a high-energy level inside the N-type element through the cold junction. At the same time, the transport electrons carry the absorbed heat (Q_C) to the hot junction, which is at temperature T_h. This heat is dissipated (Q_h) in the heat sink, while the electrons return at a lower energy level in the P-type semiconductor (the Peltier effect). If there is a temperature difference between the cold junction and hot junction of N-type and P-type thermo-elements, a voltage (called Seebeck voltage) directly proportional to the temperature difference is generated (Hrushabh *et al*., 2019).

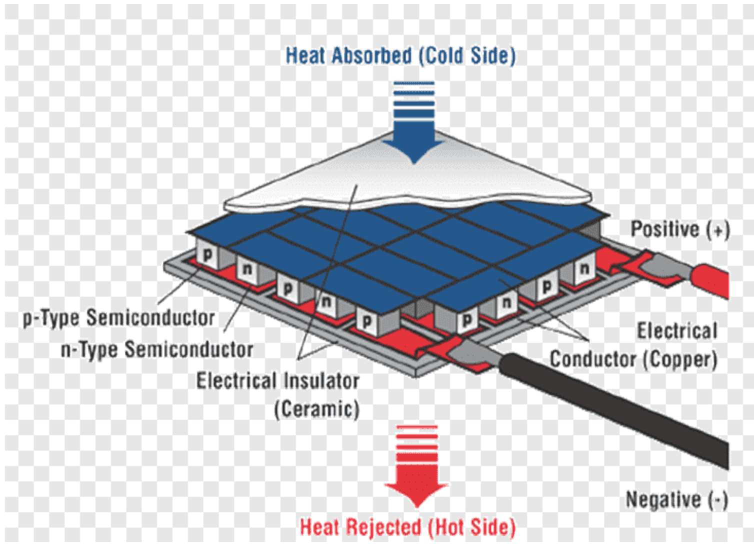

Figure 2.5: Sectional view of a thermoelectric module (Willfahrt, 2014).

The quality of a TEC cooler depends on (Sarbu & Dorca, 2018) the:

- Electric current I applied at the thermocouple of N-type and P-type thermos-elements,
- Temperatures T_h and T_c of the hot and cold sides,
- Electrical contact resistance R between the cold side and the surface of the device,
-Thermal and electrical conductivities (k, σ) of the thermo-element
- Characteristics and performance of a TEC are described by parameters like the figure of merit, the cooling capacity, and the COP.

2.2.1.2. Characteristics and performance of TEC

1. Thermoelectric figure of merit

The thermoelectric figure of merit Z, in K^{-1}, indicates if a material is a good TEC. It is an important term used to describe thermoelectric materials. It is denoted by (Sarbu & Dorca, 2018);

$$Z = \frac{\alpha^2}{\rho k} \tag{2.5}$$

Where ρ is the electrical resistivity of the material and k is the thermal conductivity. The units of Z are $1/K$. The higher the figure of merit, the better-suited material is for applications. This term relates the power production capabilities of the material to its electrical and thermal properties. The ideal thermoelectric material would have a large Seebeck coefficient and low thermal conductivity and electrical resistance. A material such as this would allow current to flow freely through it while maintaining a large thermal gradient. Typically, the figure of merit is multiplied by the absolute temperature to obtain the non-dimensional figure of merit or ZT value. Currently, ZT values are about one for most thermoelectric materials (Cooke, 2018).

ZT represents the efficiency of the N-type and P-type materials that compose a thermo-element. A thermoelectric material having a higher figure of merit ZT is more convenient, as it can carry out higher cooling power or temperature drop. Semiconductor materials are promising for the construction of thermocouples because they have Seebeck coefficients above 100 μVK^{-1}. The only way to reduce k without affecting α and ρ in bulk materials, thereby increasing ZT, is to use semiconductors of high atomic weight, such as Bi_2Te_3 and its alloys with Sb, Sn, and Pb. The figure of merit of a semiconductor material limits the temperature difference between the hot and cold sides, while the length-to-area ratio for N-type and P-type semiconductor materials defines the cooling capacity (Sarbu & Dorca, 2018).

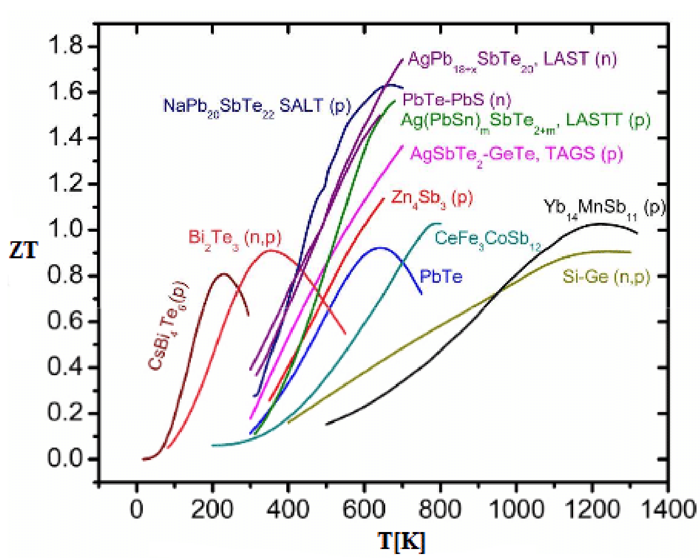

Figure 2.6: ZT versus T for different thermoelectric materials (Siouane *et al*., 2016).

The best commercial thermoelectric materials currently have ZT values around 1.0. The highest ZT value in research is about three (Sarbu & Dorca, 2018).

2. Cooling capacity

The standard simplified energy equilibrium model for thermo-element is based on the balance of heat transfer and thermoelectric effects. Assumptions have been made that:

(i) Thermoelectric material properties are temperature independent

(ii) Half of the Joule heat goes to the hot side, while the other half goes to the cold side.

From the energy balance at the cold side of the thermoelectric cooler results, the cooling capacity Qc (Huang et al., 2000; Sarbu & Dorca, 2018) as:

$$Qc = \alpha I T_c - 0.5 R_e I^2 - K\Delta T \qquad (2.6)$$

Where, R_e is the total electrical resistance given by (Vetrivel & Mohhammed Shafee, 2015):

$$R_e = \frac{\rho L_1}{A_1} + \frac{\rho L_2}{A_2} \qquad (2.7)$$

The total thermal conductance in W/K is (Gillott et al., 2010):

$$K = \frac{k_1 A_1}{L_1} + \frac{k_2 A_2}{L_2} \qquad (2.8)$$

Where,

The $\alpha I T_c$ term in equation (2.6) is the Peltier effect cooling at the thermos-element cold side depending on the Seebeck coefficient α, the input current I, and the temperature of the cold junction Tc;

The $0.5 R_e I^2$ term in equation (2.6) is the Joule heat, which depends on the electrical resistance R_e of the thermo-elements in series and the input current I;

The $K\Delta T$ term in equation (2.6) is the heat flux conducted from the hot junction to the cold junction (according to Fourier law) that depends on the thermal conductance k of the thermocouple and the temperature difference between hot and cold sides, $\Delta T = T_h - T_c$;

k is the thermal conductivity;

ρ is the electrical resistivity;

A and L represent the cross-sectional area and the length of the thermoelectric element, respectively.

The subscripts 1 and 2 refer to the thermoelectric materials 1 and 2, respectively.

3. Coefficient of performance

The COP of a thermoelectric cooler can be calculated as follows (Sarbu & Dorca, 2018):

$$COP = \frac{Q_c}{W} \tag{2.9}$$

Where Q_c is the cooling capacity and W is the electrical power consumption of the thermoelectric cooler given by

$$W = RI^2 + \alpha I \Delta T \tag{2.10}$$

Combining equations (2.6), (2.9), and (2.10) into account, the COP of the thermoelectric module is given by

$$COP = \frac{Q_c}{W} = \frac{\alpha I T_c - 0.5 R_e I^2 - K\Delta T}{RI^2 + \alpha I \Delta T} \tag{2.11}$$

There exists an optimum current for maximum COP if T_h and T_c, and the thermoelectric material are settled. Solving the equation $\partial COP/\partial I = 0$, the optimum current for the maximum (optimum) COP can be given by;

$$I_{opt} = \frac{\alpha \Delta T / R_e}{\sqrt{1 + Z\overline{\overline{T}}} - 1} \tag{2.12}$$

Where, $Z\overline{T}$ is the thermoelectric material figure of merit at average hot and cold side temperature, $\overline{T} = \frac{T_h + T_c}{2}$. Replacing I in equation (2.11) by I_{opt}, the optimum COP can be given by:

$$COP_{max} = \frac{T_c}{T_h - T_c} \frac{\sqrt{1 + Z\overline{\overline{T}}} - (\frac{T_h}{T_c})}{\sqrt{1 + Z\overline{\overline{T}}} + 1} \tag{2.13}$$

In the design of a thermoelectric cooling system, one has to take into account both the system *cooling power* output and *cooling COP* with consideration of both the thermoelectric module performance and the heat sink design. Therefore, thermoelectric cooling system design is a compromise between the cooling capacity and COP.

The COP of a thermoelectric module can be improved by:

1. Optimizing the heat dissipation
2. Reducing the electrical contact and thermal resistances
3. Use new materials, e.g., with negative Thomson effect.
4. Use multistage modules.

2.2.2. The advantages of a thermoelectric module

The advantages of the module are no moving parts so maintenance is easier, does not pose the danger of carbon, temperature regulation can be more flexible, smaller in size than regular cooling, and setting it easier for just changing a voltage or current input (Sunawar & Garniwa, 2017).

Advantages of thermoelectric cooling over conventional AC system are (Singh, 2015):

1. Weight: thermoelectric units weigh 1/3 to 1/2 as much as the other units because of the lightweight cooling system and lack of a heavy compressor unit.
2. Compactness: thermoelectric is the most compact system because of the small size of the cooling components.
3. Price: thermoelectric coolers cost 20%-40% less than the equivalent sized compressor
5. Safety: thermoelectric systems are completely safe because they use no gases or open flames and run on just 12 volts. Compressor systems can leak Freon, which can be extremely dangerous especially if heated.
6. Battery drain: thermoelectric coolers have a maximum current drain of 12 volts of 4.5 amps. Compressor portables draw slightly more current when running but may average slightly less depending on thermostatic control settings.
7. Ease of servicing and maintenance: thermoelectric units have only one moving part, a small fan (and 12-volt motor) which can easily be replaced with only a screwdriver. Most parts are easily replaced by the end-user. Compressor and absorption units both require trained (expensive) mechanics and special service equipment to service them.

8. Cooling performance: compressor systems are potentially the most efficient in hot weather. Some models will perform as a portable freezer and will refrigerate in ambient temperatures of up to 110 degrees F. thermoelectric units will refrigerate in sustained ambient temperatures of up to 95 degrees F.

9. Reliability: thermoelectric modules do not wear out or deteriorate with use. They have been used for military and aerospace applications for years because of their reliability and other unique features. Compressors and their motors are both subject to wear and Freon-filled coils are subject to leakage and costly repairs. (Singh, 2015).

Pache *et al*. (2014) has stated that thermoelectric Refrigeration &Air conditioning technology will overcome all the disadvantages of the existing A/C system. Conventional A/C system has many disadvantages like the use of hazardous refrigerants, bulky system, orientation problems, etc. The new A/C system using thermoelectric couple which shall overcome all the disadvantages of existing A/C system which gives advantages like environment-friendly, precise temperature control, spot cooling, compact, high reliability, electrically quiet operation, ability to heat and cool with the same module. The most widely used thermoelectric material in the temperature range of 120℃ to 230℃ is a pseudo-binary alloy, $(BiSb)_2(TeSe)_2$, commonly referred to as bismuth telluride. For normal thermoelectric devices, the maximum temperature difference between the hot and cold sides can reach 70℃. Large temperature differentials (up to 130℃) can be achieved by multistage series. The lowest practically achievable temperature is about $-100℃$. This system has no moving parts and therefore, needs substantially less maintenance; the life of these devices exceeds 100,000 hours of steady-state operation, it can function in environments that are too severe, too sensitive, or too small for a conventional R & A/C system.

Rawat (2013) has designed and developed an experimental thermoelectric refrigeration system having a refrigeration space of 1 liter. Cooling is achieved by using four thermoelectric cooling modules ($Q_{max} = 19W$) and a heat sink fan assembly ($R_{th} = 0.50\ ℃/W$) for each thermoelectric module which is used to increase heat dissipation rate. A temperature reduction of 11℃ without any heat load and 9℃ with 100 ml of water in refrigeration space for 23℃ ambient temperature has been experimentally found in the first 30 minutes at optimized operating conditions. The calculated COP of the thermoelectric refrigeration cabinet was 0.1.

Rawat *et al*. (2013) has developed some prototype thermoelectric refrigerators with different heat exchanger combinations and evaluated their cooling performances in terms of COP, heat-pumping capacity, cooling down rate, and temperature stability. The COP of the refrigerator is found to be 0.3-0.5 for a typical operating temperature of 5℃ with ambient at 25℃. The potential improvement in the cooling performance of a thermoelectric refrigerator is also investigated employing a realistic model with experimental data. The results show that an increase in its COP is possible through improvements in module contact resistance, thermal interfaces, and the effectiveness of heat exchangers.

Vella *et al*. (2012) have shown that a thermoelectric generator, which draws its heat from solar energy, is a particularly suitable source of electrical power for the operation of a thermoelectric refrigerator. They developed the theory of the combined thermoelectric generator and refrigerator and determined the ratio of the numbers of thermocouples needed for the 2 devices. A 4-couple thermoelectric generator has been used to power a single-couple refrigerator.

Shams *et al*. (2016) presented the design and implementation of a novel, low-cost solar-powered car cooling system for idle parked cars. This system is targeted towards Gulf countries such as the United Arab Emirates as high ambient temperature changes may cause interior damage to the car and pose a significant burn threat for babies, disabled or elderly people. The main motive of the system was to decrease the temperature inside the parked car as much as possible to make a significant difference for the driver and the passengers. The cooling system consisted of brushless motors such that the hot air would be blown out from the car and the interior is cooled. It comprised a thermoelectric cooling device (TEC), heat sink, and three brushless motors. Its power consumption was about 240 W. The main components are solar panel, DHT11 Temperature Sensor (for measuring cabin temperature), digital thermometer (for measuring ambient temperature), relay, microcontroller (Arduino UNO), etc. The system was tested on a car prototype made of wood while its windows are made of good insulating material and it could decrease the cabin temperature from 27℃ to 23℃ in 15 minutes.

K & Joy (2020) proposed an original solution for cabin heat removal from parked cars by using an intelligent solar modulated system equipped with Peltier modules. It was a thermoelectric system composed of two pairs of Peltier modules, a solar panel, and four pairs of cross-flow fans. The Peltier modules, placed under the car roof cabin between the steel plate and the indoor insulation, and the fans are placed just under the roof indoor insulation. The cabin was exposed to sun radiation (600-800 W/m^2) with no wind. Indoor temperature was measured with no ventilation. The data was used to design the positions of Peltier modules. A prototype made of the following selected materials as a square tube (0.5 inches), G I sheet (2 mm), G I sheet (5 mm), Glass (4 mm). Solar panel: 12 V, 120W solar panel (Luminous), Thermocouple: K type thermocouple (2 Nos.*)* The car roof was cut, and all the Peltier modules were placed at different locations. A heat sink and fan were fixed on the hot side of the module. Similarly, a fan was fixed at the cold side of the module. The indoor temperature was measured with no ventilation and was found to be lower than the ambient temperature.

Mohiuddin *et al*. (2019) focused on ways to reduce the interior temperature of the parked vehicle. A system had been designed that employs the solar panel, battery, inlet and exhaust fans, temperature sensor, and an electric control circuit. The experiment was performed on a car cabin prototype of a model made using the CPU casing of a desktop computer. The inlet air fan is located lower than the exhaust air fan in the car model because hot air moves up and to have a better airflow distribution. It was observed that the interior temperature of the car model decreased significantly when the system was installed. The simulation was done by using ANSYS FLUENT R15 to investigate the airflow distribution inside the car cabin when inlet and outlet fans were in action. The results showed that the car interior has a better airflow distribution when the inlet fan is positioned lower than the outlet fan.

John *et al*. (2014) fabricated a solar-powered heat control system to control the temperature of a parked car. The principle of this system is based on Newton's law of cooling. Two micro high-efficiency fans are fitted into the system to circulate air in and out of the parked car and act as an inlet and outlet. The micro fan draws in air, which later passed through a closed chamber containing acetone as a liquid coolant. The fans are electrically powered using solar panels based on the solar energy controlling principle. The result indicated that the temperature inside the car cabin increased rapidly for the first 5 minutes when the system was installed with acetone coolant. Then, it decreased with constant steps to the next 10 minutes and remained constant. The system manifested an average of 8.40℃ reduction of temperature within a short interval and it runs completely on green energy.

2.3. General Considerations in Designing Car Cabin Cooling System

The air-conditioned vehicle must work under varying conditions of ambient temperature, latitude, passenger load, etc. In deciding the capacity of the system, certain assumptions regarding some different conditions should be made.

The following factors should be considered to design a vehicle cabin cooling system:

- ✓ Changes in regional microclimates caused by local geography along the Automobile's route
- ✓ Thermal stratification (vertical air temperature variation)
- ✓ The velocity of the air and or the automobile
- ✓ Radiation effects of windows and other structures.
- ✓ Variation of solar heat load due to the changing solar orientation.

Thermal comfort is influenced by:

- ✓ Personal factors (degree of activity, clothing, journey time)
- ✓ Spatial factors (radiant temperature, temperature of vehicle enclosing surface or body)
- ✓ Ventilation factors (air temperature, airspeed, relative humidity)

The above factors must be considered to achieve cabin thermal conditions which will be perceived as comfortable by a majority of passengers (Tadesse, 2015).

Temperature variations

Depending on the type influencing conditions, the temperature balance in the passenger compartment can change rapidly. Because it is highly impractical to accurately simulate these dynamic conditions in a test environment, evaluation of these criteria is best made under stabilized conditions with all doors closed for the duration of the evaluation measurements.

Temperature variations inside a parked car

The temperature rise in a parked vehicle is mainly due to solar radiation and greenhouse effect. Solar radiation enters through the glasses and it is partially trapped within the car. The measured temperature inside a parked car on a summer day (June) in Aswan, (Egypt) could reach 120℃ where the outside temperature is ranging from 35℃ - 45℃. The measurements take place at different conditions of closed and opened windows of a parked car. The car was parked and exposed to direct sunray at free air all day in Aswan (latitude 24, longitude 32). The car was divided into four sections dashboard, front seats, rear seats, and rear board. Four identical thermometers are fixed on each section to measure the temperature during the time. The temperature is measured when the car was closed, lowering the driver's window by 1 cm, lowering the front two windows by 1 cm, lowering the four windows by 1 cm, lowering the four windows by 3 cm, and covering the front and rear glasses with a car sunshade. The time of the maximum cabin temperature (about 120 ℃) is quite close to the time of the maximum of the outside air (about 40℃) (Abdel-Fadeel *et al*., 2014).

The temperatures of front and rear boards are always greater than that of front and rear seats. This is because the largest amount of solar radiation passes into the car when the largest projected area of glass is facing the sun's rays. The wind speed inside the car is very small to reduce the temperature inside the car. (Abdel-Fadeel *et al*., 2014).

Al-Kayiem *et al*. (2010) had conducted experimental and numerical analyses on the thermal accumulation and distribution in the interior of a parked vehicle. The experimental data were taken from measurements of six different cases consisting of full windows closing, four different window opening settings, and usage of sunshade. The temperatures at 12 different locations were recorded. Among all the measurements inside the car, the spot near the glass windshields recorded the highest temperature.

Quadri and Jose (2013) studied computational analysis of thermal distribution within the passenger car cabin during parking. The 3D car cabin model was simulated using FLUENT 6.3.26. To determine the intensity of radiations falling on the windowpanes, a solar calculator has been used. Slits with specific dimensions were cut on the model, cold air was allowed to enter the cabin to represent the inlet, and outlet vents in a car. The areas around the windowpanes experienced the highest temperatures when the solar radiations fell on them and a porous slit positioned above the windows could act as a vent for hot air. The simulation proved that the location of the vents plays a vital role in determining the cabin environment and the velocity inlets can reduce the high thermal accumulation due to the incoming solar radiations.

2.4. Literature Summary and Research Gaps

From the literature review, it can be summarized as the areas around the front glass windshield and rear glass window of car cabins experience the highest temperature. The existing A/C system is unable to perform during parking as it is based on the engine's power. Running the conventional A/C through solar power is not feasible because of the high-power requirement of the system. Therefore, designing a car cabin cooling system using a thermoelectric device is possible but increasing its efficiency should be the main concern. Although different studies had been conducted to reduce the cabin temperature of a parked vehicle, an optimal design of the selection of the solar panel and the number of thermoelectric modules based on the obtainable solar-electric energy for a specific vehicle type has not been done. In addition to this, the cooling system was controlled by an on/off switch, which could be manually operated. To cool the cabin temperature quickly, in a conventional A/C car, the passenger/driver should either wait for some time or let the A/C run. This leads to a waste of resources (time and fuel). Therefore, this solar-powered car cabin cooling system should operate on its own based on the temperature sensor installed inside the cabin to increase thermal comfort. Therefore, the aim of this thesis is designing of a solar-powered automatic thermoelectric cooling for automobile cabins to reduce the cabin temperature.

CHAPTER THREE

MATERIALS AND METHODS

In this chapter, the materials and devices used for the thesis work are listed. The materials and tools used for demonstrating the thermoelectric cooling system are listed and the methods followed to conduct the thesis are also indicated.

3.1. Materials

Materials that are used for conducting this study are:

Measuring devices: for measuring the temperatures of cabin air, car surfaces, car windshield glasses, etc. E.g. K-type thermocouple thermometer, DHT11 sensor.
Cutting and shaping tools: for making car models for the demonstration. E.g., cutter, grinder, hammer, driller, and scissors.
Metering devices: to measure the length, width, and thickness of aluminum heat sinks, aluminum sheet metals, carton insulating materials. E.g., Meter, Vernier caliper.
Fastening devices: for making the demo and joining its components.

Software used for the thesis work are:

Modeling software: for 3D modeling of the car cabin. E.g., CATIA V5 R20.
Simulating software: for simulating aerodynamic CFD analysis. E.g., ANSYS FLUENT 19.3.
Computing software: for computing design calculations. E.g., Mathcad prime 7.

3.2. Methods

The necessary data required for this study are collected from primary and secondary sources. Different pieces of literature, journals, handbooks, etc are used to conduct this study. After having collected the necessary data, the total heat gain by the car cabin from different heat sources is analytically estimated. Theoretical approaches are used. Internal and external heat sinks, and thermoelectric cooler are designed. Circuit design and simulation are done using proteus and Arduino software. The aerodynamic effect of the thermoelectric cooling system on the car is also simulated using ANSYS FLUENT software. Finally, the automatic thermoelectric cooling system is practically demonstrated. The methods followed for designing the automatic thermoelectric cooling system are shown in Figure 3.1 below.

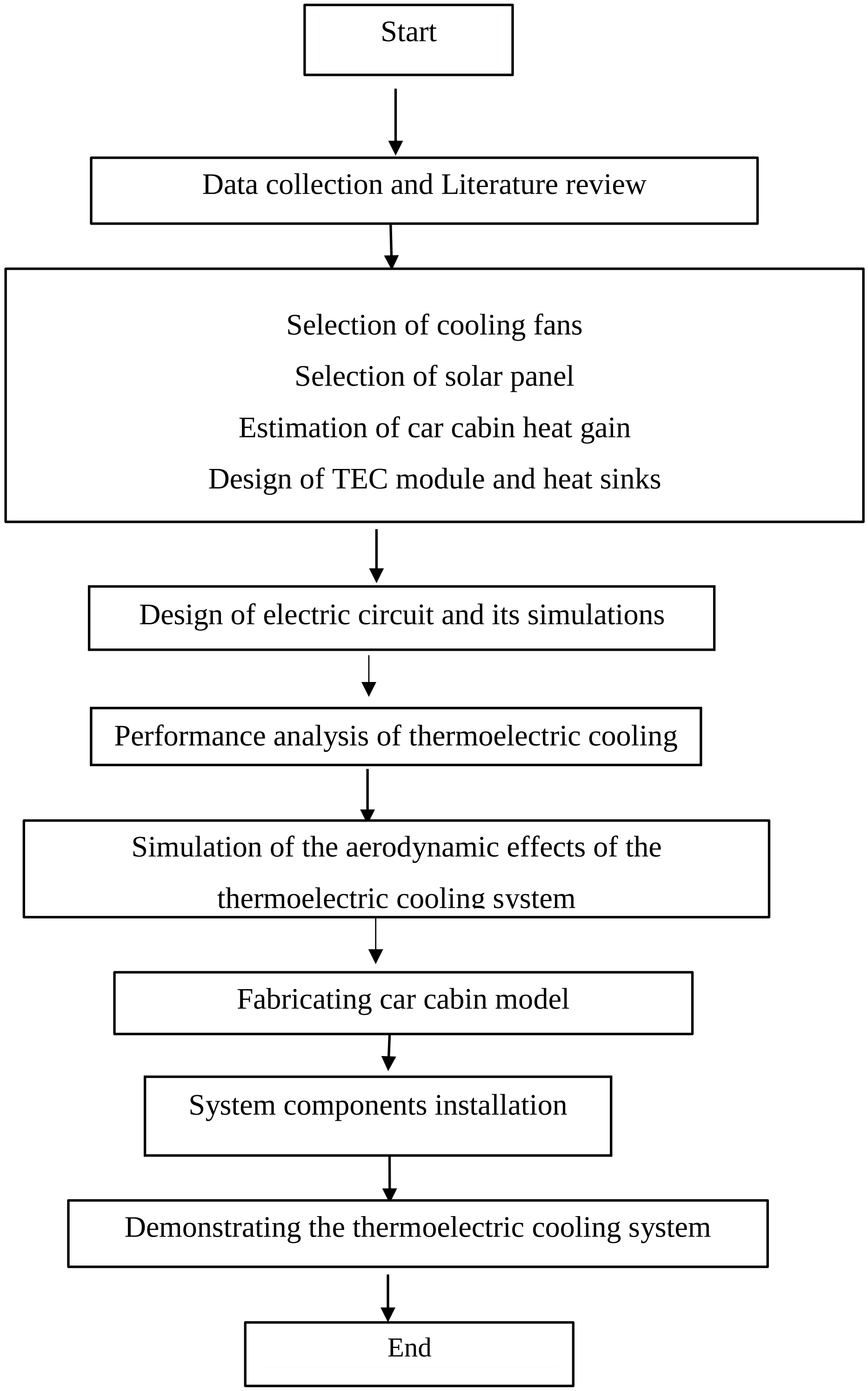

Figure 3.1: Flow diagram of the methodology

3.2.1. Data collection

To calculate the thermal load or the net heat gain by the cabin the required data have been collected from different pieces of literature, journals, books, and the internet. Furthermore, primary data from direct measurement has been collected. Inside surface temperature, cabin temperature, and outside surface temperature of Toyota Vitz car exposed to direct sunlight on a solar noon, have been recorded and the car was. Additionally, the approximate dimension of the car cabin (especially the outer surface dimension) is measured directly using a meter and Vernier caliper.

The temperature test was conducted using a K-type thermocouple thermometer at 5 places inside the cabin and outside of the cabin (outer surface body). Since Adama (Ethiopia) is located in the northern hemisphere the car was parked facing south so that it receives maximum solar radiation through front windshield glass. Note that maximum solar radiation enters the cabin through front windshield glass. The main aim of the test was to estimate the maximum cabin air and surface temperature of the car during parking. The experimental test on the Toyota Vitz car held on March 29, 2021, at Adama city is presented in Table (C.3).

To estimate the thermal load of the car cabin solar radiation estimation is necessary. Therefore, six-year (2015-2020) solar data is collected from the Adama meteorology agency.

3.2.2. Estimation of solar radiation

The amount of solar radiation falling on a surface on Earth is calculated using multiple correlations that relate radiation outside the earth's atmosphere (extraterrestrial radiation) to radiation inside the earth's atmosphere (interplanetary radiation) (terrestrial radiation). The geometric relationship between a plane located on Earth and the incoming solar radiation, that is, the position of the sun relative to that plane, must first be calculated to undertake solar radiation analysis. Several angles can be used to determine this relationship (Tadele, 2020).

Fundamental sun-earth angles

The major angles that describe the geometric relationship between the earth and the incoming solar radiation from the sun are (Tadele, 2020):

1. Latitude (ϕ): the angular location north or south of the equator, north positive; $-90° \leq \phi \leq 90°$. The latitude of Adama is 8.54° north of the equator.

2. Declination (δ): the angular position of the sun at solar noon with respect to the plane of the equator, north positive; $-23.45° \leq \delta \leq 23.45°$.

$$\delta = 23.45 \times sin(\frac{360(284+n)}{365}) \tag{3.1}$$

Where n is the day of the year (counted from January 1).

3. Slope or tilt angle (ε): the angle between the inclined plane surface under consideration and the horizontal; $-180° \leq \varepsilon \leq 180°$.

4. Hour angle (ω): the angular displacement of the sun east or west of the local meridian due to the rotation of the earth on its axis at 15° per hour; positive in the afternoon and negative in the forenoon.

$$\omega = [\text{solar time} - 12{:}00]\ (\text{in hours}) \times 15° \tag{3.2}$$

5. Zenith angle (θ_z): it is the angle between the vertical and the line to the sun, that is, the angle of incidence of beam radiation on a horizontal surface.

$$\text{Cos}\ \theta z = \cos\delta \cos\phi \cos\omega + \sin\phi \sin\delta \tag{3.3}$$

6. Surface azimuth angle (γ): the deviation of the projection on a horizontal plane of the normal to the surface from the local meridian. $\gamma = 0$ for surfaces facing south. For tilted surfaces in the northern hemisphere facing south, west, north, and east, surface azimuth angle, γ = 0, -90,180 and 90 respectively.

7. Angle of incidence (θ): the angle between the sun's rays is incident on the plane surface and normal to that surface.

$$\begin{aligned} \cos\theta = {} & \sin\delta \sin\phi \cos\varepsilon \quad \sin\delta \cos\phi \sin\varepsilon \cos\gamma + \cos\delta \cos\phi \cos\varepsilon \cos\omega \\ & + \cos\delta \sin\phi \sin\varepsilon \cos\gamma \cos\omega + \cos\delta \sin\varepsilon \sin\gamma \sin\omega \end{aligned} \tag{3.4}$$

a. **Estimation of daily extraterrestrial radiation on a horizontal surface**

The extraterrestrial radiation on a surface normal to the sun's rays kept at the actual sun-earth distance at a specific day and time, which is modified to take into account the varying distance between the sun and the earth, is determined by (Duffie and Beckman, 2013):

$$I_{ext} = I_{sc}\,[1.0 + 0.033 cos(\frac{360(n)}{365})] \tag{3.5}$$

Where, n is the day of the year (counted from January 1) and I_{sc} is solar constant =1367 W/m^2.

Extraterrestrial solar radiation that would fall on a horizontal surface at the location is given by:

$$I_o = I_{ext} \cos \theta z \tag{3.6}$$

$$I_o = I_{sc}\,[1.0 + 0.033\cos(\frac{360(n)}{365})][\cos\delta \cos\phi \cos\omega + \sin\phi \sin\delta] \tag{3.7}$$

The daily extraterrestrial solar radiation on a horizontal surface can be obtained by integrating equation (3.3) from sunrise to sunset and expressed as:

$$H_o = \frac{24\times3600}{\pi} I_{sc}\,[1.0 + 0.033\cos(\frac{360(n)}{365})][\cos\delta \cos\phi \sin\omega_{sr} + \frac{\pi\times\omega_{sr}}{180} \sin\phi \sin\delta] \tag{3.8}$$

Where, sunset hour angle

$$\omega_{sr}=\cos^{-1}(\tan\phi \tan\delta) \tag{3.9}$$

b. **Estimation of monthly average daily global radiations on a horizontal surface**

The first empirical correlation for the estimation of global solar radiation was proposed by Angstrom. The correlation relates the radiation with the number of sunshine hours in a day using empirical constants obtained by regression analysis. The well-known Angstrom relation for estimating the monthly average daily solar radiation on a horizontal surface is given as (Tadele, 2020):

$$\frac{H_G}{H_o} = a_1 + b_1\,(\frac{\bar{n}}{\bar{N}}) \tag{3.10}$$

Where, H_G is monthly average daily global solar radiation in the terrestrial region, $\bar{n}$ and $\bar{N}$ are the daily and maximum possible daily hours of bright sunshine,

a_1 and b_1 are regression coefficients given by,

$$a_1 = -0.11 + 0.235 \cos \phi + 0.32 \left(\frac{\bar{n}}{\bar{N}}\right) \quad (3.11)$$

$$b_1 = 1.449 - 0.533 \cos \phi - 0.694 \left(\frac{\bar{n}}{\bar{N}}\right) \quad (3.12)$$

c. Estimation of monthly average daily diffuse and beam radiations on a horizontal surface

The monthly average daily diffuse radiation on a horizontal surface can be determined from the monthly average daily global radiation on a horizontal surface and the number of bright sunshine hours and is given by the correlation (Tadele, 2020):

$$\frac{H_d}{H_G} = 0.931 - 0.814\left(\frac{\bar{n}}{\bar{N}}\right) \quad (3.13)$$

The monthly average daily beam radiation on a horizontal surface is the difference between the monthly average daily global and diffuse radiations.

$$H_b = H_G - H_d \quad (3.14)$$

d. Estimation of monthly average hourly global radiation on a horizontal surface

The monthly average hourly global radiation on a horizontal surface can be determined from the monthly average daily global radiation (Duffie and Beckman, 2013) as shown in Figure 3.2.

$$\frac{I_G}{H_G} = \frac{\pi}{24}(a_2 + b_2 \cos \omega)\left(\frac{\cos \omega - \cos \omega_{sr}}{\sin \omega_{sr} - \frac{\pi}{180}\,\omega_{sr} \cos \omega_{sr}}\right) \quad (3.15)$$

Where,

$$a_2 = 0.409 + 0.5016 \sin(\omega_{sr} - 60) \quad (3.16)$$

$$b_2 = 0.6609 - 0.4767 \sin(\omega_{sr} - 60) \quad (3.17)$$

e. Estimation of monthly average hourly diffuse and beam radiations on a horizontal surface

The monthly average hourly diffuse radiation on a horizontal surface can be determined from the monthly average daily diffuse radiation on a horizontal surface (Duffie and Beckman, 2013) and presented in Figure 3.3.

$$\frac{I_d}{H_d} = \frac{\pi}{24}\left(\frac{\cos\omega - \cos\omega_{sr}}{\sin\omega_{sr} - \frac{\pi}{180}\,\omega_{sr}\cos\omega_{sr}}\right) \tag{3.18}$$

The monthly average hourly beam radiation on a horizontal surface is the difference between the monthly average hourly global and diffuse radiations as shown in Figure 3.4.

$$I_b = I_G - I_d \tag{3.19}$$

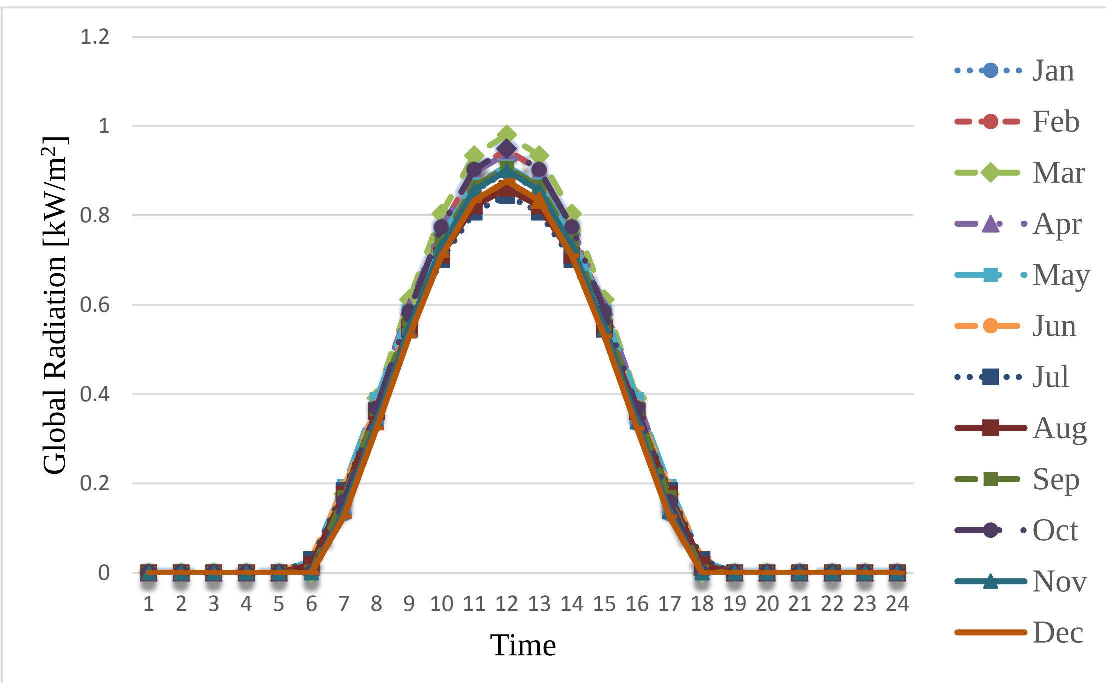

Figure 3.2: Monthly average hourly global solar radiation on a horizontal surface.

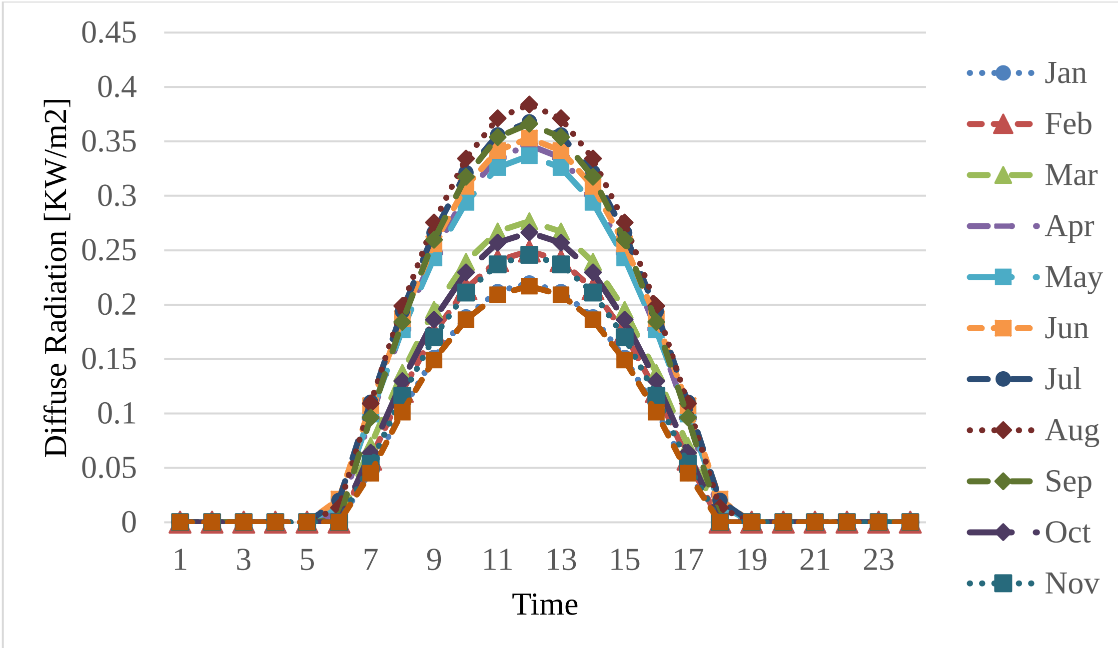

Figure 3.3: Monthly average hourly diffuse radiation on a horizontal surface.

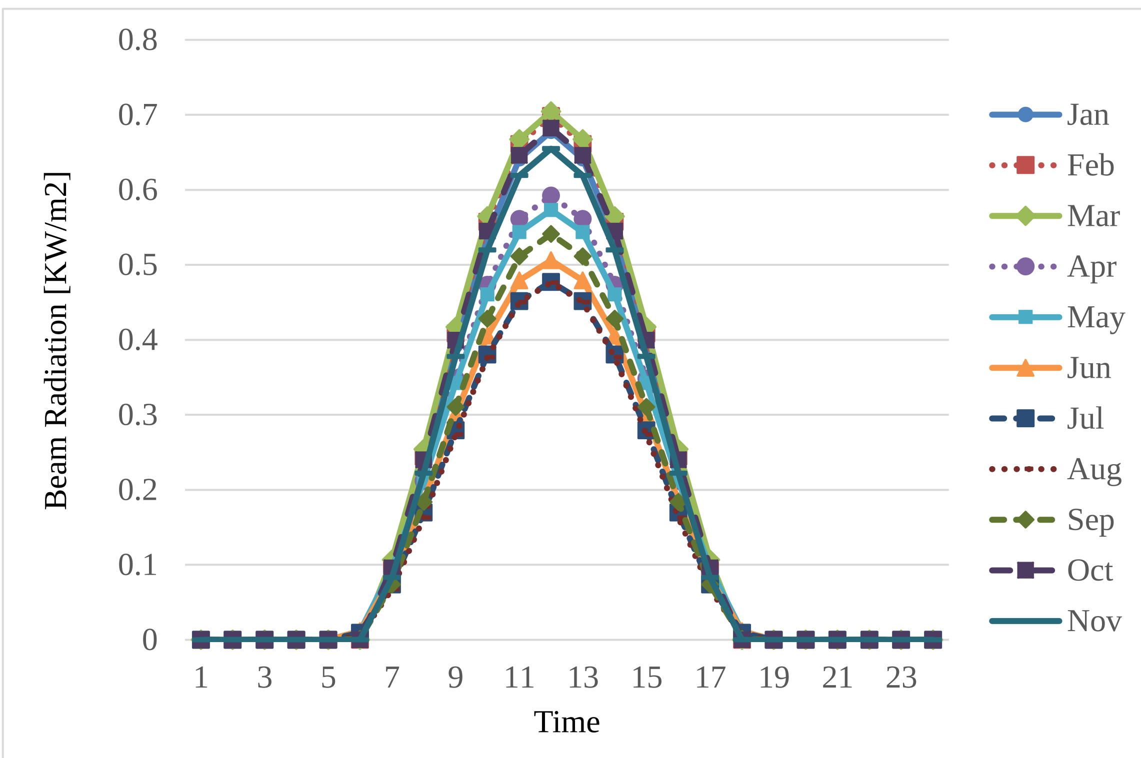

Figure 3.4: Monthly average hourly beam (direct) solar radiation on a horizontal surface

Estimation of incident solar radiation on a tilted surface

The incident solar radiation on an inclined surface is the sum of the beam, diffuse and reflected solar radiation from various surfaces (from a horizontal surface and surfaces surrounding it). Therefore, the total incident solar radiation on a surface tilted at an angle ε can be expressed in terms of the direct (beam), diffuse and the total reflected radiation to the tilted surface (Duffie and Beckman, 2013).

$$I_{Total} = I_{Dir} + I_{Dif} + I_{Ref} \tag{3.20}$$

Where,

I_{Dir} is the direct/beam incident radiation

I_{Dif} is the diffuse incident radiation

I_{Ref} is the reflected incident radiation

Direct, diffuse, and reflected incident radiation for tilted surfaces can be calculated by (Tadele, 2020; Vaghela & Kapadia, 2014);

$$I_{Dir} = I_b R_b \tag{3.21}$$

$$I_{Dif} = I_d \left(\frac{1+ \cos \varepsilon}{2}\right) \tag{3.22}$$

$$I_{Ref} = I_G \rho_g \left(\frac{1- \cos \varepsilon}{2}\right) \tag{3.23}$$

Where, R_b is the beam radiation factor, and it can be defined as the ratio of the incident beam radiation on a tilted surface to that on a horizontal surface.

$$R_b = \frac{\cos \theta}{\cos \theta_z} \tag{3.24}$$

Where, ρ_g is the reflectivity of ground and its value is 0.2 for ordinary ground (Tadele, 2020).

CHAPTER FOUR

DESIGN OF THERMOELECTRIC COOLING SYSTEM

In this chapter, a selection of cooling fans and solar panel is done. Heat sinks and thermoelectric cooler module has also been designed. The design of the electric circuit and its simulation for the automatic thermoelectric cooling system is also performed. The Aerodynamic effect of the cooling system is evaluated using ANSYS FLUENT. The car cabin thermoelectric cooling is also demonstrated.

4.1. Description of the Thermoelectric Cooling System

The schematic of the automatic thermoelectric cooling system is given in Figure 4.1. It consists of a 12V solar panel with solar charge controller, a 12v battery, DC-DC step-down voltage regulator, DHT11 temperature and humidity sensor, Arduino Uno, TEC modules, heat sinks, and cooling system, etc.

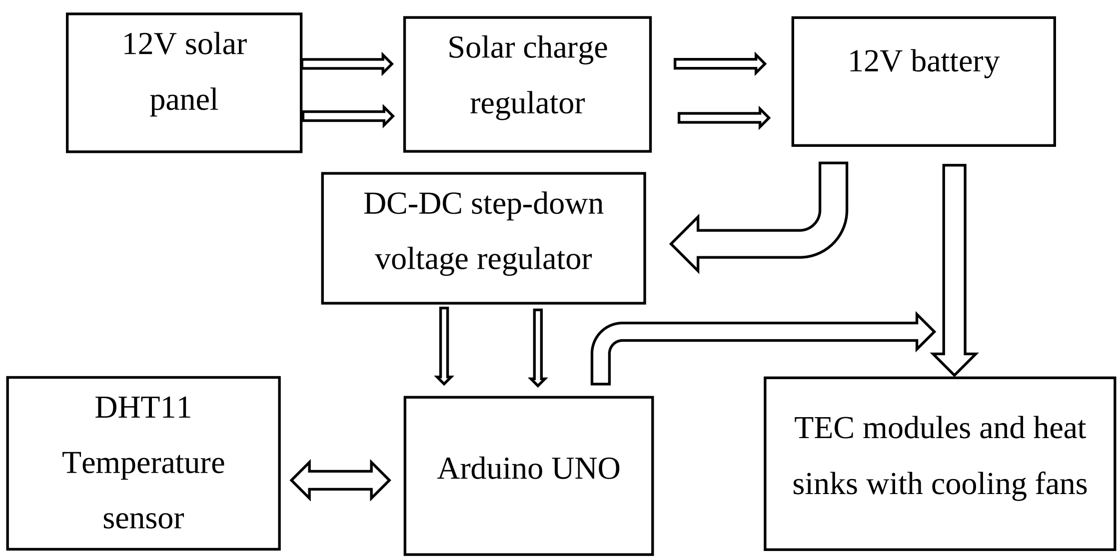

Figure 4.1: Schematic diagram of automatic thermoelectric cooling system

Components of the cooling system

The components of the automatic thermoelectric cooling system are a thermoelectric cooler module, heat sink, and cold sink, cooling fans, solar panel with power controller/ regulator, rechargeable battery/ car battery, Arduino, temperature sensor, transistor, etc.

Thermoelectric cooler module: - The number, type, and specifications of the TEC module required for the system is determined through the design processes. The minimum specifications for selecting an appropriate TEC by the designer must be based on the following parameters;

- ✓ Cold side temperature (T_c)
- ✓ Hot side temperature (T_h)
- ✓ Operating temperature difference (ΔT), which is the temperature difference between T_h and T_c
- ✓ Amount of heat to be absorbed in the TEC's cold surface. This can also be termed as heat load. It is represented as (Q) and the unit is Watts
- ✓ Operating current (I) and operating voltage (V) of the TEC.

Figure 4.2: Peltier's TEC module

Heat sink: - The dimensions of the heat sink and cold sink which are used as the heat exchanger are determined through the design process of the cooling system.

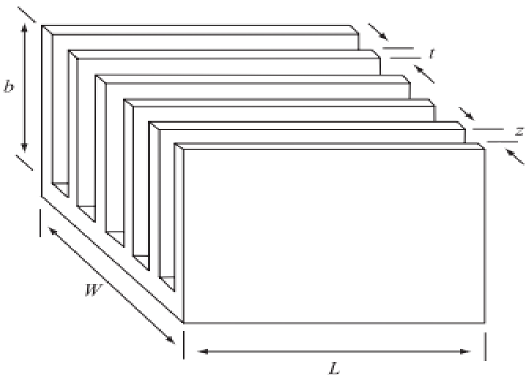

Figure 4.3: Rectangular multiple fins heat sink (Wiley, 2011).

Cooling Fans: - CPU cooling fans are used for the thermoelectric cooling system. The dimensions for the common cooling fans range from 40 mm × 40 mm to 120 mm × 120 mm. The smaller the cooling fan the lower is its volume flow rate. The larger the cooling fan the more surface area it covers and the higher its aerodynamic drag coefficient is. To compromise the two parameters, for outer cooling fans, an 80 mm × 80 mm cooling fan is selected. For the aerodynamic drag, the fan thickness should be as small as possible. Therefore, it is better to compare different case fans to select the required one as follows (https://www.frozencpu.com).

Table 4.1: Selection criteria for the external cooling fans

Parameters	Fan models		
	1 Cooljag F128038BU	2 Delta NMB-MAT 3112KL-04W-B69	3 SUNON KD1208PTBX- 6(2)318.AF.GN
Flow rate (CFM)	56.66	58.6	50.6
Dimension (mm)	80 × 80 × 38	80 × 80 × 32	80 × 80 × 25
Noise level (dB (A))	45.5	44	40.5
Power input (W)	6	6.96	4.3

Based on the selection criteria of smaller fan thickness, low noise level, and low power consumption, model number 3 has been selected for the external fans of the cooling system.

For the internal heat sink, we take a cooling fan with dimensions as small as possible to hold a little space in the cabin. Fan thickness more matters for the internal cooling fans. The volume flow rate of the fan also has relations with its loudness. This is because as the cfm of a fan increases the louder it is.

From Table 4.2, the cooling fan with the lowest noise level and operating power is selected for the internal cooling fans. I.e. model number two.

Table 4.2: Selection criteria for the internal cooling fans

Parameters	Fan models		
	1 FAN7X10TX3	2 AV-F7010	3 FD127010MB
Flow rate (CFM)	21.33	13.31~19.13	35.3
Dimension (mm)	70 × 70 × 10	70 × 70 × 10	70 × 70 × 10
Noise level (dB (A))	33	32.68	41.5
Power input (W)	2.16	1.74	3.12

Solar panel with power controller/ regulator: - Due to the limited space available on the roof of the car, the size of the solar panel is limited. The approximate surface area of the roof of a Toyota Vitz/Yaris 2008 car is 1.7 m × 1.1 m. Therefore, solar panel size with the cooling system is restricted to this dimension. High solar power is to be generated within this specified area of the surface. The solar panel specified below is more advantageous than others by its both dimension and high wattage.

The special advantage of this panel is that since it is flexible it can be installed over the car's roof surface without or with some roof modification.

Figure 4.4: A 175 W flexible solar panel

[https://www.renogy.com/175-watt-12-volt-flexible-monocrystalline-solar-panel/]

Table 4.3: Specifications of the 175 W flexible solar panel

Maximum power	175 W	Operating temperature	-40 ℃ - 85 ℃
Open circuit voltage:	23.9 V	Optimum operating current:	8.98 A
Dimensions (mm):	$1503.68 \times 673.10 \times 2.03$	Short circuit current (I_{sc}):	9.50 A
Optimum operating voltage:	19.5 V	Weight (kg):	2.81
		Power output:	95%

Rechargeable battery/ car battery: - Depending on the voltage, power, current requirement, and capacitance, at least a 69.27 amp hr 12V rated battery is needed for the cooling system.

Arduino microcontroller: - To control the auto mode of the thermoelectric cooling system an Arduino controller is needed. It reads the cabin temperature from the temperature sensor installed in the cabin and decides whether the cooling system should be turned on/off comparing the preset comfort temperature and the temperature read from the sensor/s. Arduino UNO is selected, as it is a common device for many purposes.

Temperature sensor: - To determine the cabin air temperature, a temperature sensor is required. Selection is based on their temperature range, accuracy, response time, stability, linearity, and sensitivity of the sensor. For the best accuracy, the DHT11 temperature sensor is selected. It is low-cost and operates best between temperatures of zero to 50 degrees Celsius.

DC-DC step-down voltage convertor: - For the temperature sensor, 5 V power is needed. To get this power source from the 12-volt battery we must use a step-down voltage converter. Here, the LM2596 voltage converter is selected.

Transistor: - The transistor is an electrical device, which can be used as a switch to control a large electrical current with a small base current. The on and off modes of the TEC module and fans are controlled by the Arduino controller through the transistor. Since the TEC module draws up to a 6 A current, the transistor to be used here needs to have a collector current of 6 A or more. TIP120 transistor is selected.

Configurations of the components of the thermoelectric cooling system.

The outer cooling fans are installed on the outer roof surface of the car followed by the external heat sinks. In the middle, the TEC is placed so that it is in contact with both the external and internal heat sinks. The internal heat sinks are installed under the roof surface/ceiling in the cabin. The car roof is made to have a rectangular hole for placing the thermoelectric cooler module. The internal cooling fans are installed over the internal heat sinks at the bottom side. Figure 4.2 shows the configuration of the components of the thermoelectric cooling system.

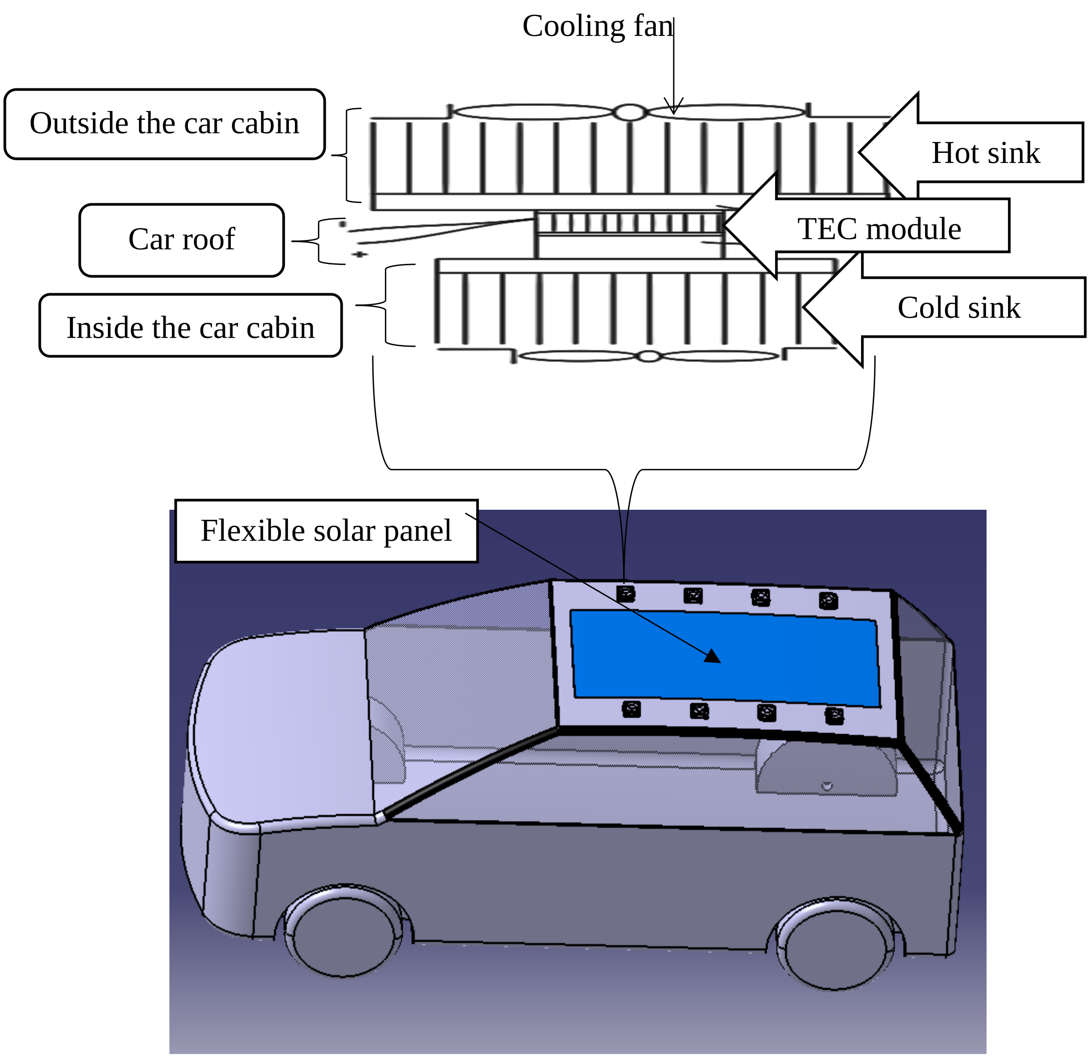

Figure 4.5: Configuration of TEC module, heat sinks, and cooling fans for the cooling system

4.2. Estimation of the Cooling Load of the Car Cabin

The cooling load is the amount of heat energy that needs to be removed from a space to maintain the desired temperature. To determine the cooling load the total heat gain to the cabin must be estimated.

Heat gain calculation

The net heat gain by the vehicle cabin during parking can be classified under the following categories. The total load, as well as each of these loads, can either be positive (heating the cabin) or negative (cooling down the cabin). The summation of all the load types will be the instantaneous cabin overall heat load gain. Mathematically, it can be expressed as (Vaghela & Kapadia, 2014);

$$Q_{Tot} = Q_{Dir} + Q_{Dif} + Q_{Ref} + Q_{Amb} \tag{4.1}$$

Where,

Q_{Tot}, is the net overall thermal load encountered by the car cabin,

$Q_{Dir,}$ is direct load and Q_{Dif} is diffuse load,

$Q_{Ref,}$ is reflected radiation load and Q_{Amb} is ambient load.

Material properties for the car body are indicated in Table 4.5. The necessary data for estimation of the thermal loads are also presented in the next Table 4.4.

Table 4.4: Specifications /data concerning the calculations (Tadele, 2020)

Month	March
Time	12:00 AM – 1:00 PM
Location	Adama, Ethiopia
Latitude	8°44' North Latitude and 39°04' East Longitude
Ground reflectivity	0.2
Ambient temperature	30℃
Initial cabin temperature	46°C
Comfort temperature	24℃

Table 4.5: Material properties for the car body (Fayazbakhsh & Bahrami, 2013).

Properties	Glass	Vehicle body
Conductivity (W/m.K)	0.8	0.2
Density (kg/m^3)	2500	1500
Transmissivity	0.5	0
Absorptivity	0.3	0.4
Specific heat (J/kg.K)	840	1000
Thickness (mm)	3	-

1. Radiation heat load

The heat gain due to solar radiation is a significant part of the cooling loads encountered in vehicles. According to (Vaghela & Kapadia, 2014; Vinofer, 2016) solar radiation heat load can be categorized into direct, diffuse, and reflected radiation loads.

a) Direct radiation

It is that part of the incident solar radiation which directly strikes a (horizontal) surface of the vehicle body, which is calculated from (Fayazbakhsh & Bahrami, 2013; Vaghela & Kapadia, 2014);

$$Q_{Dir} = \sum A\tau I_{Dir}\cos\theta \tag{4.3}$$

Where I_{Dir} the direct incident radiation heat gain per unit area and θ is the incidence angle between the surface normal and the position of the sun in the sky. τ is the surface element transmissivity and A is the surface area, respectively.

Before local sunrise and after local sunset, simply no radiation loads are considered. According to the climate data from the meteorological agency of Ethiopia, the hottest months in most parts of Ethiopia are March, April, and May. In this paper, the calculation of the radiation heat load is based on March.

The monthly average hourly incidences of beam/direct radiation on a horizontal surface in March month is (Figure 3.4):

$$I_b = 704\ W/m^2$$

The direct solar radiation heat gain for front windshield glass, rear windshield glass, right side window glasses, and left side window glass can be determined as:

Table 4.6: Measured data (except surface azimuth angle) for calculations

	Front windshield	Rear windshield	Right side glass	Left side glass
Surface area (m^2)	0.91	0.44	0.505	0.505
Tilt angle (°)	25	65	65	65
Surface azimuth angle (°)	0	180	-90	90

Using the given values from Table 4.6 and combining equations (3.3), (3.4), (3.21), (3.24) and (4.3), we have direct radiation heat gain through front windshield glass:

For front windshield glass: Q_{Dir}= 307.53 W.

For rear windshield glass: Q_{Dir}= 40.28 W.

For right side window glasses: Q_{Dir}= 52.89 W.

For left side window glasses: Q_{Dir}= 52.89 W.

For vehicle cabins other than glasses, Q_{Dir} is zero as their transmissivity is zero.

Total direct heat gain through the vehicle glass Q_{Dir} is equal to;

$$Q_{Dir} = 453.59 \text{ W}$$

b) Diffuse radiation

It is the part of solar radiation, which results from indirect radiation of daylight on the surface. During a cloudy day, most of the solar radiation is received from this diffuse radiation. The diffuse radiation heat gain is calculated by (Vaghela & Kapadia, 2014);

$$Q_{Dif} = \sum A\tau I_{Dif} \tag{4.4}$$

Where, I_{Dif} is the diffuse radiation heat gain per unit area.

However, $I_{Dif} = 276.67\ W/m^2$ (Figure 3.3). Combining equations (3.22) and (4.4) gives the diffuse radiation heat gain:

For front windshield glass, $Q_{Dif} = 119.96$ W.

For rear windshield glasses, $Q_{Dif} = 43.27$ W.

For right side window glasses, $Q_{Dif} = 49.66$ W.

For left side window glasses, $Q_{Dif} = 49.66$ W.

Total diffusion radiation heat gain to the cabin across the car glasses is the sum of diffuse radiation heat gain via each of the glasses.

$$Q_{Dif\_total} = 262.55\ W$$

c) Reflected radiation

It refers to the part of radiation heat gain, which is reflected from the ground and strikes the body surfaces of the vehicle. The reflected radiation is calculated by (Vaghela & Kapadia, 2014);

$$Q_{Ref} = \sum A\tau I_{Ref} \tag{4.5}$$

Where, I_{Ref} is the reflected radiation heat gain per unit area.

Combining equations (3.23) and (4.5) gives the reflected radiation heat gain via the car glasses:

For front windshield glass, $Q_{Ref} = 4.10$ W.

For rear windshield glasses, $Q_{Ref} = 12.43$ W.

For right side window glasses, $Q_{Ref} = 14.26$ W.

For left side window glasses, $Q_{Ref} = 14.26$ W.

Total Q_{Ref} is equal to: $Q_{Ref} = 45.05$W.

The total heat gain by the vehicle cabin (glasses) from solar radiation is equal to the sum of the direct, diffuse, and reflected components of the radiation heat gain.

$$Q_{Rad} = 761.19\ W.$$

2. Ambient Load

The ambient load is the contribution of the thermal load transferred to the cabin air due to the temperature difference between the ambient and cabin air. Exterior convection, conduction through body panels, and interior convection are involved in the total heat transfer between the ambient and the cabin (Abdulsalam *et al.*, 2007; Vaghela & Kapadia, 2014).

$$Q_{Amb} = \sum AU\left(T_s - T_i\right) \tag{4.6}$$

Where U is the overall heat transfer coefficient of the surface element. T_s and T_i are the average surface temperature and average cabin temperature, respectively. U has different components consisting of inside convection, conduction through the surface, and outside convection. It can be written in the form (Vaghela & Kapadia, 2014);

$$U = 1/R \tag{4.7}$$

Where, *R* is the net thermal resistance for a unit surface area expressed as:

$$R = \frac{1}{h_0} + \frac{\chi}{k} + \frac{1}{h_i} \tag{4.8}$$

Where, h_o and h_i are the outside and inside convection coefficients, *k* is the surface thermal conductivity, and χ is the thickness of the surface element. The thermal conductivity and thickness of the vehicle surface can be measured rather easily. The convection coefficients h_o and h_i depend on the orientation of the surface and the air velocity. Here, the following estimation is used to estimate the convection heat transfer coefficients as a function of vehicle speed (Abdulsalam *et al.*, 2007; Vaghela & Kapadia, 2014);

$$h = 0.6+6.64\left(V\right)^{0.5} \tag{4.9}$$

Where,

h is the convection heat transfer coefficient in W/m^2K and

V is the vehicle speed in *m/s*.

Despite its simplicity, this correlation is applicable in all practical automotive instances. The cabin air is assumed stationary and the ambient air velocity is considered equal to the vehicle velocity. This implies that

h_i = 0.6 but, for h_o, ambient air speed = 1.33 m/s (from metrological data) can be considered as V. Ideally, the heat transfer from the surface of the car body to the cabin air when the car is traveling is less than the heat transfer when the car is parked. Because during traveling there is more outside convection related to the high speed of the car. Note that on a sunny day the un-shaded surface temperature of the car is larger than the ambient air. Therefore, the heat gain calculation focuses on a parked condition.

For glasses:

k = 0.8 W/mK, χ = 0.003 m, A = 2.36 m^2

Combining equations (4.7), (4.8) and (4.9), the overall thermal conductivity of glasses is:

$$U = 0.6\ W/m^2K$$

From the temperature test result average outer surface temperature of glasses (all glasses on the vehicle body) is taken as 46^0c and cabin air temperature as 24^0 c. substituting these values in the equation (4.6) gives;

$$Q_{g,Amb} = 31.15W.$$

For surfaces:

k = 0.2W/mK, χ = 0.05 m (assuming average surface thickness) and A = 6.41 m^2

Using equations (4.7), (4.8), and (4.6):

$$Q_{S,Amb} = 69.38\ W.$$

The total heat gain from the ambient air to the cabin is 100.53W.

Table 4.7: Summary of car cabin thermal load during parking

Heat load	Unit (W)
Q_{Rad}	761.19
Q_{Amb}	100.53
Total	861.72

4.3 Design of Heat Sinks

To visualize the energy flow in the entire system, a thermal circuit is constructed. R_i and R_o are the overall thermal resistances for the internal heat sink and external heat sink, respectively. The components of the air cooler are an internal heat sink, a thermoelectric module, and an external heat sink as shown in Figure 4.6. Q_c is the amount of heat transported at the internal heat sink, which is the design requirement. Applying an energy balance or first law of thermodynamics to the system gives a relationship as:

$$Q_c = Q_h - W$$

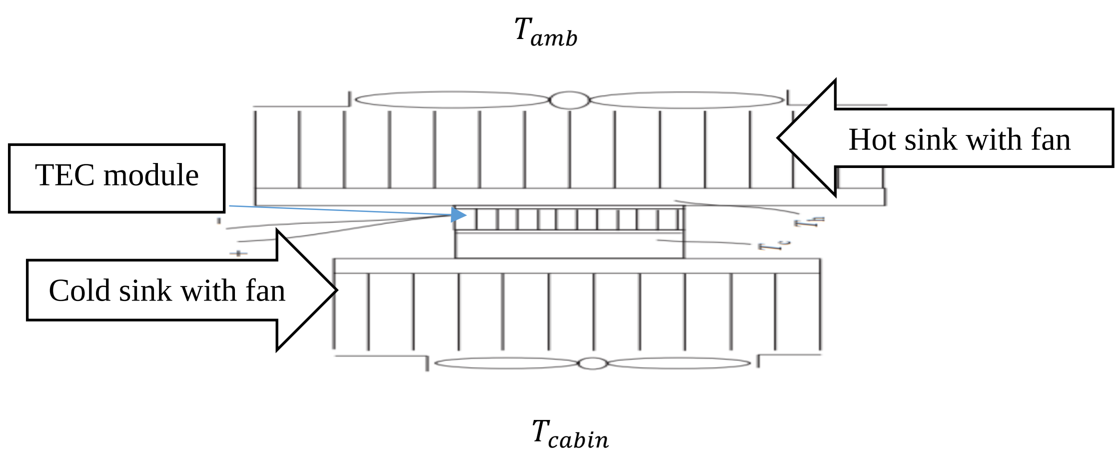

a)

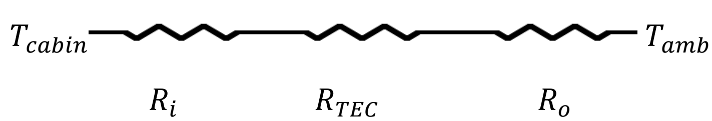

b)

Figure 4.6: (a) Schematic of air cooler, (b) Thermal circuit of the cooler

This indicates that Q_h is Q_c plus W. This is the reason why the external heat sink appears larger than the internal heat sink. T_h is usually assumed approximately 15 ℃ higher than the ambient temperature so that it allows the heat dissipation to be possible. Tc is also approximately 15 ℃ lower than the internal air temperature for the same reason. The smaller the temperature difference, the greater the heat flow or the *COP* is to be expected (Wiley, 2011). According to Raut *et al*. (2012) for a natural and forced convection heat sink, delta T at the hot sides should be between 20 ℃ to 40 ℃ and 10 ℃ to 15 ℃ respectively. With these initial assumptions on T_c and T_h, the internal and external heat sinks are designed, eventually formulating the heat transfer equations as a function of T_c and T_h.

Based on the availability and less weight of the materials for the heat sinks, although, copper is more conductive, aluminum is selected due to the compromise of listed parameters. Due to the available space in the cabin roof ceiling of the car, the internal heat sink and fans must occupy as small space as possible. Since the cold air must be dispersed to increase convective heat transfer between the cabin air and the heat sink, CPU cooling fans are used.

The rate of heat transfer depends on heat sink dimension, material, and fin thickness. In this paper, the dimensions of the heat sink and the volume flow rates for the fans are made fixed and proceeded to design optimum fin thickness for the maximum heat transfer.

The following design is based on the Wiley (2011) thermal design book. For the design optimization, *Mathcad prime 7* software is used.

Subscript 1 and 2 denotes the internal heat sink (cold sink) and external heat sink, respectively.

Assumptions:

1. The radiation heat transfer is negligible.
2. The fluid is considered incompressible with constant properties (air).
3. The heat source is assumed to be generating a uniform temperature with time.
4. There is no contact resistance where the base of the fin joins the prime surface.
5. The convective heat transfer coefficient on the faces of the fin is constant and uniform over the entire surface of the fin

The geometry of the internal and external heat sinks:

Width: $W_1 = 70\ mm,\quad W_2 = 80\ mm,$ Length: $L_1 = 70\ mm,\quad L_2 = 80\ mm$

Fin height: $b_1 = 5\ mm,\quad b_2 = 5\ mm$

The internal and external air temperatures and the cold and hot junction temperatures are estimated now and updated later.

$$T_{comf} = 297.15\ K,\ \ T_C = 283.15\ K,\ \ \Delta T_1 = T_{comf} - T_C = 14\ K$$

$$T_h = 318.15\ K, T_{amb} = 303.15\ K,\quad \Delta T_2 = T_h - T_{Amb} = 15\ K$$

The properties of air at the film temperatures at (T_c + T_{comf})/2 and (T_h + T_{amb})/2 (Table A.1) by extrapolation gives;

$$K_{air1} = 0.0255\ W/mK \qquad V_{air1} = 15.0 \times 10^{-6}\ m^2/s \qquad P_{air1} = 0.7096$$

$$K_{air2} = 0.02707\ W/mK \qquad V_{air2} = 16.946 \times 10^{-6}\ m^2/s \qquad P_{air2} = 0.7055$$

The properties of aluminum are obtained from Table A.2 as

$$\rho_{Al} = 2702\ \frac{kg}{m^3} \qquad k_{Al} = 237\frac{W}{m.K}$$

4.3.1. Design of internal and external heat sinks with cooling fans at both sides

CPU case fans having the following volume flow rates are used

$$V_{fr1} = 16.22\ cfm \qquad V_{fr2} = 50.6\ cfm$$

The cross-flow areas and the velocities (perpendicular flow divided by two) are;

$$A_{c1} = b_1.W_1$$

$$A_{c2} = b_2.W_2, \tag{4.10}$$

$$U_1 = \frac{1}{2}\frac{V_{fr1}}{A_{c1}}$$

$$U_2 = \frac{1}{2}\frac{V_{fr2}}{A_{c2}} \tag{4.11}$$

The characteristic length for flow over a fin plate is length divided by 2, assuming, that the perpendicular flow by a fan takes half of the total length.

$$\mathrm{L}_{c1} = \frac{L_1}{2}$$

$$\mathrm{L}_{c2} = \frac{L_2}{2} \tag{4.12}$$

The Reynolds numbers show laminar flows (less than 10×10^5) (Wiley, 2011).

$$R_{e1} = U_1 \cdot \frac{L_{c1}}{V_{air1}}$$

$$R_{e2} = U_2 \cdot \frac{L_{c2}}{V_{air2}} \tag{4.13}$$

The optimum fin spacing is found using the following Equation (Wiley, 2011):

$$Z_{opt1} = 3.24 L_{c1} R_{e1}{}^{\frac{-1}{2}} P_{rair1}{}^{\frac{-1}{4}}$$

$$Z_{opt2} = 3.24 L_{c2} R_{e2}{}^{\frac{-1}{2}} \times P_{rair2}{}^{\frac{-1}{4}} \tag{4.14}$$

The average heat transfer coefficients for laminar flow are (Wiley, 2011);

$$h_1 = 0.664 \frac{K_{air1}}{L_{c1}} R_{e1}{}^{\frac{1}{2}} P_{rair1}{}^{\frac{1}{3}}$$

$$h_2 = 0.664 \frac{K_{air2}}{L_{c2}} R_{e2}{}^{\frac{1}{2}} P_{rair2}{}^{\frac{1}{3}} \tag{4.15}$$

The number of fins is obtained as a function of fin thickness to find the optimum fin thickness (Wiley, 2011).

$$n_{f1}(t_1) = \frac{W_1}{Z_{opt1} + t_1}$$

$$n_{f2}(t_2) = \frac{W_2}{Z_{opt2} + t_2} \tag{4.16}$$

The mass of fins is (Wiley, 2011):

$$m_{f1}(t_1) = n_{f1}(t_1) \rho_{Al} L_1 b_1 t_1$$

$$m_{f2}(t_2) = n_{f2}(t_2) \rho_{Al} L_2 b_2 t_2 \tag{4.17}$$

We have the thermal expansion coefficients:

$$\beta_1(t_1) = b_1 \left(\frac{2h_1}{K_{Al} t_1}\right)^{\frac{1}{2}}$$

$$\beta_2(t_2) = b_2 \left(\frac{2h_2}{K_{Al} t_2}\right)^{\frac{1}{2}} \tag{4.18}$$

The single fin efficiency is found using (Wiley, 2011);

$$\eta_{f1}(t_1) = \frac{\tanh(\beta_1(t_1))}{\beta_1(t_1)}$$

$$\eta_{f2}(t_2) = \frac{\tanh(\beta_2(t_2))}{\beta_2(t_2)} \tag{4.19}$$

The single fin areas are (Wiley, 2011):

$$A_{f1}(t_1) = 2(L_1 + t_1)b_1$$

$$A_{f2}(t_2) = 2(L_2 + t_2)b_2 \tag{4.20}$$

The total surface areas are obtained considering the single fin area and the inter-fins area (Wiley, 2011).

$$A_{t1}(t_1) = n_{f1}(t_1)(A_{f1}(t_1) + L_1 Z_{opt1})$$

$$A_{t2}(t_2) = n_{f2}(t_2)(A_{f2}(t_2) + L_2 Z_{opt2}) \tag{4.21}$$

The overall efficiency is obtained using (Wiley, 2011);

$$\eta_{o1}(t_1) = 1 - n_{f1}(t_1)\frac{A_{f1}(t_1)}{A_{t1}(t_1)}(1 - \eta_{f1}(t_1))$$

$$\eta_{o2}(t_2) = 1 - n_{f2}(t_2)\frac{A_{f2}(t_2)}{A_{t2}(t_2)}(1 - \eta_{f2}(t_2)) \tag{4.22}$$

Now, the total heat transfers are obtained as (Wiley, 2011):

$$q_{tot1}(t_1) = \eta_{o1}(t_1)A_1(t_1)h_1\Delta T_1$$

$$q_{tot2}(t_2) = \eta_{o2}(t_2)A_2(t_2)h_2\Delta T_2 \tag{4.23}$$

The overall thermal resistances are obtained using (Wiley, 2011):

$$R_{tot1}(t_1) = \frac{1}{\eta_{o1}(t_1)h_1A_{t1}(t_1)}$$

$$R_{tot2}(t_2) = \frac{1}{\eta_{o2}(t_2)h_2A_{t2}(t_2)} \tag{4.24}$$

Combining all equations from equation (4.10) to equation (4.24) along with the given data, the optimum fin thickness is found using Mathcad's built-in function of '**Solve block**' as follows:

Guess:

$$t_1 := 1\,mm \qquad\qquad t_2 := 1\,mm$$

$t_1 := maximize(q_{tot1}, t_1)$

$$t_1 = 5.821 \times 10^{-5}\,m \qquad\qquad q_{tot1}(t_1) = 56.99\,W$$

$$n_{f1}(t_1) = 81.166 \qquad\qquad m_{f1}(t_1) = 0.005\,kg$$

$$\eta_{o1}(t_1) = 0.932 \qquad\qquad R_{tot1}(t_1) = 0.246\,\frac{s^3.K}{kg.m^2}$$

$$Z_{opt1} = 0.8\,mm$$

$t_2 := maximize(q_{tot2}, t_2)$

$$t_2 = 6 \times 10^{-5}\,m \qquad\qquad q_{tot2}(t_2) = 162.63\,W$$

$$n_{f2}(t_2) = 134.9 \qquad\qquad m_{f1}(t_1) = 0.009\,kg$$

$$\eta_{o2}(t_2) = 0.897 \qquad\qquad R_{tot2}(t_2) = 0.092\,\frac{s^3.K}{kg.m^2}$$

$$Z_{opt2} = 0.53\,mm$$

The heat transfer rates in the internal and external heat sinks for the optimum fin thickness based on the assumptions of T_c and T_h can be updated with their exact solution, which is to be obtained later.

4.3.2. Design of internal and external heat sinks with no cooling fans at both sides

From Table (A.1), effective thermal diffusivity $\alpha = 97.1 \times 10^{-6}$ m²/s.

Thermal expansion coefficient is given by: $1/T_{film}$

$$\beta_1 = \frac{1}{290}\,K^{-1}$$

$$\beta_2 = \frac{1}{310.5}\,K^{-}1 \qquad (4.25)$$

Nusselts number and Rayleigh number for natural convection over a horizontal plate of Ra < 10^7 is given by (Maragkos, 2021):

$$Ra_1 = \frac{g\beta_1 \Delta T_1}{\alpha V_{air1}} {L_1}^3$$

$$Ra_2 = \frac{g\beta_2 \Delta T_2}{\alpha V_{air1}} {L_2}^3 \tag{4.26}$$

$$Nu_1 = 0.54 Ra_1 Ra_1^{1/4}$$

$$Nu_2 = 0.54 Ra_2 Ra_2^{1/4} \tag{4.27}$$

Characteristic length for horizontal plate is (Maragkos, 2021):

$$L_{c1} = \frac{L_1 W_1}{2(L_1 + W_1)}$$

$$L_{c2} = \frac{L_2 W_2}{2(L_2 + W_2)} \tag{4.28}$$

Optimum fin spacing for the heat sink (Wiley, 2011):

$$Z_{opt1} = 2.714 L_{c1} Ra_1^{-1/4}$$

$$Z_{opt2} = 2.714 L_{c2} Ra_2^{-1/4} \tag{4.29}$$

The heat transfer coefficient is determined by **(**Wiley, 2011; Maragkos, 2021)

$$h_1 = \frac{K_{air1}}{L_{c1}} Nu_1$$

$$h_2 = \frac{K_{air2}}{L_{c1}} Nu_2 \tag{4.30}$$

The rest procedures and formulas are similar to part (a). Table 4.8 summarizes the heat sink design with natural convection at both sides.

Table 4.8: Summary of the heat sink design with natural convections

	Internal heat sink	External heat sink
Q_{cmax}	4.619	-
$Q_h(W)$	-	6.06
Fin thickness (mm) for Q_{cmax}	0.046	0.05
Fin spacing (mm)	3	3
Number of fins	26	28
Heat sink resistance (K/W)	3.031	2.473
Efficiency	0.983	0.985
Mass of fins (g)	1	2

4.3.3. Design of internal and external heat sinks with only external cooling fans

We now consider the cooling power and heat sink parameters for the cooling system that encompasses only the outer fans or excluding the internal fans. For the same dimension of both

Table 4.9: Design result for the heat sinks without internal fans

	Internal	External
Q_C (W)	7.95	-
$Q_h(W)$	-	144
Fin thickness (mm) for Q_{cmax}	0.217	0.2
Fin spacing (mm)	5	1
Number of fins	12.768	65
Heat sink thermal resistance (m^2K/W)	1.773	0.105
Efficiency	0.962	0.84
Mass of fins (gm)	15	7

internal and external heat sinks following the same design procedure as the above sections. Table (4.9) is the results for the heat sinks with no internal cooling fans.

Evaluation of the cooling system without internal heat sinks but with internal fans

On the internal side of the cooling system, let us now use only internal fans. I.e. the cabin air is directly in contact with the cold side of the thermoelectric module (TEC).

If TEC1-12706 is taken, the active cooling surface area A is 39mm by 39mm. From newton's law of cooling, the amount of heat absorbed into the Peltier module can be determined as

$$Q_C = h \times A \times (\Delta T) \tag{4.31}$$

However, for the value of convective heat transfer coefficient, h, we can take the value calculated in (a), which is 66.284 W/m^2K. Moreover, assume the cabin air is at its maximum temperature of 46 ℃, ΔT between the cold side of the TEC module and cabin air is 36 ^{0}c.

$$Q_C = 2.639 \text{ W}$$

As we see, the value of Q_C is very low. It is because of the low convective cooling area of the Peltier module.

As we have seen above, the best design of heat sink for cooling is the design (a). Hence, the TEC module will be designed based on the heat sink design of condition (a).

4.4 Design of Thermoelectric Cooler Module

For the design purpose, *Mathcad software* is used for the calculations and different kinds of literature (journals and textbooks) on thermoelectricity are also used.

Because of its high figure of merit at low temperatures between 270 K and 350 K (Siouane *et al*., 2016), bismuth telluride material has been selected for the design**.**

Assumptions:

1. There is no electrical contact resistance between thermo-elements and no thermal resistance between ceramic plates and the electrical contact.
2. The junction temperatures are assumed to be steadily maintained
3. Thermos-physical properties such as resistivity, conductivity, etc., do not change with temperature.
4. Heat transfer takes place only through the P-type and N-type semiconductor

5. The convection and radiation heat losses are negligible.
6. The Thomson effect is negligible. It has been proven analytically and experimentally that the Thomson effect has a very small effect on the performance of TEG and TEC (Mani, 2016).

The TEC material of Bismuth telluride (Bi_2Te_3) is used having the following properties (Wiley, 2011);

$$\alpha_p = -\alpha_n = 200\ \mu V/K, \quad \alpha_p - \alpha_n = 400\ \mu V/K, \quad \rho_p = \rho_n = 1.0 \times 10^{-5} \Omega m$$

$$\rho_p + \rho_n = 2.0 \times 10^{-5} \Omega m, \quad k_p = k_n = 1.52\ \frac{W}{mK}, \quad k_p + k_n = 3.04\ \frac{W}{mK}$$

The cold and hot side junction temperatures are taken as the same as for the heat sinks.

$$T_h = 318.15\ K \qquad T_C = 283.15\ K$$

The cross-sectional area and leg length of the thermo-element are:

$$A_e = 2.6\ mm^2 \qquad L_e = 2\ mm$$

The same number of thermocouples is adopted as a typical module:

$$n = 127$$

The temperature difference between the cold and hot junctions is defined as;

$$\Delta T = T_h - T_c$$

The figure of merit from equation (2.5) is;

$$Z = 0.003\ K^{-1}$$

The internal resistance R_e and the thermal conductance k_e of a thermocouple are calculated using equations (2.7) and (2.8) as;

$$R_e = 0.015\ \Omega \qquad k_e = 0.004\ W/mK$$

There are three design criteria for the TEC module (Wiley, 2011):

1. Design based on the maximum cooling power
2. Design based on the maximum COP and

3. Design based on the midpoint of the current between the maximum cooling power and maximum COP of the TEC module.

They all are considered and finally the last one is chosen, as the cabin cooling system needs both the optimized power and cooling capacity.

4.4.1. Design based on the maximum cooling power

The current for the maximum cooling power is (Wiley, 2011);

$$I_{maxp} = \frac{\alpha T_c}{R} = 7.362\ A$$

Multiplying equation (2.6) by the number of thermo-elements gives the maximum cooling power.

$$Q_{cmaxp} = 36.49\ W$$

Multiplying equation (2.10) by the number of thermo-elements n results in the power input

$$W_{maxp} = 116.33\ W$$

Using equation (2.9), the *COP* at the maximum cooling power is calculated as;

$$COP_{max} = \frac{Qc}{W} = 0.31$$

4.4.2. Design based on the maximum COP

The dimensionless figure of merit (Siouane et al., 2016);

$$Z\bar{T} = Z\frac{Th+Tc}{2} = 0.791$$

Using equation (2.12), the current for the maximum *COP* is

$$I_{max.cop} = 2.75\ A$$

The maximum cooling power at the maximum coefficient of performance is calculated by multiplying equation (2.6) by the number of thermo-elements used.

$$Q_{c.max.cop} = 14.65\ W$$

The power input for the maximum coefficient of performance using equation (2.10) and multiplying by the number of thermo-elements, is;

$$W_{max.cop} = 19.40\ W$$

The *COP* using equation (2.9)

$$\mathrm{COP}_{\mathrm{max\ cop}} = \frac{\mathrm{Qc}}{\mathrm{W}} = 0.75$$

4.4.3. Design Based on the midpoint of the current between the maximum cooling power and maximum COP

Since the thermoelectric cooling system runs on solar power, both maximum cooling and low power are needed. As a result, design the cooling system based on the midpoint of the current.

The midpoint current is (Wiley, 2011);

$$I_{mid} = \frac{I_{mp} + I_{cop}}{2} = 5.6\ \mathrm{A}$$

The cooling power and power input can be calculated by multiplying equations (2.6) and equation (2.10) by the number of thermo-elements used.

$$Q_{cmid} = 30.61\ W$$

$$W_{mid} = 57.78\ W$$

The midpoint *COP* using equation (2.9) is;

$$\mathrm{COP} = 0.52$$

But, to use a 12-volt battery as a power source, the current has to be expressed in terms of the desired voltage, V_o =12 V (Wiley, 2011) as;

$$Io = \frac{\frac{Vo}{n} - \alpha\Delta T}{R} = 5.36 \text{ A}$$

Using equation (2.6) for cooling power and equation (2.10) for power input, we obtain;

$$Q_{co} = 31.97\, W$$

$$W_o = 64.39\, W$$

The heat balance gives;

$$Q_h = Q_{co} + W_o = 96.36\, W$$

The relationship between the heat sinks and the TEC is (Wiley, 2011);

$$Q_C = q_{tot1} \tag{4.32}$$

$$Q_h = q_{tot2} \tag{4.33}$$

Table 4.10 presented the results for the midpoint design.

Table 4.10: Summary of the TEC design

TEC	
Parameters	Optimum
Qc (W)	31.97
W (W)	64.39
Q_h (W)	96.36
COP	0.493
Voltage (V)	12
Current (A)	5.36
$Q_{C,max}(W)$	54.27
ΔT_{max}(K)	105.492
V_{max}(V)	19.743
I_{max} (A)	7.362

Finding the exact solution for T_c and T_h

Combining Equation (2.6) with equation (4.32) and equation (2.10) with equation (4.33) yields two equations for two unknowns, T_c and T_h. Re-write the given and estimated temperatures. Mathcad block is constructed to find the solutions as;

$$\frac{T_{cabin}-T_c}{R_{tot1}(t_1)} = n[\alpha T_c I_o - \frac{1}{2} I_o^2 R_e - k_e(T_h - T_c)] \tag{4.37}$$

$$\frac{T_h-T_{ex}}{R_{tot2}(t_2)} = \frac{T_{cabin}-T_c}{R_{tot1}(t_1)} + n[\alpha\, I_o(T_h - T_c) + I_o^2 R_e] \tag{4.38}$$

$$\begin{bmatrix} T_c \\ T_h \end{bmatrix} := Find\ (T_c, T_h) \Rightarrow \begin{bmatrix} T_c \\ T_h \end{bmatrix} = \begin{bmatrix} 287.78 \\ 312.045 \end{bmatrix} K$$

(Note: In the equation (4.37) and (4.38), the only unknowns are T_c and T_h.)

We need to update the heat transfer data with the exact temperatures obtained above**.** Using equation (2.6) and (2.10) results:

$$Q_{co} = 38.088\ W, \text{ and } W_o = 58.59\ W$$

The maximum performance parameters are obtained from the following equations (Barrubeeah et al., 2021);

$$I_{max} = \frac{\alpha T_c}{R_e}, \qquad \Delta T_{max} = 0.5Z \times T_c^2$$

$$Q_{c.max} = nk_e \Delta T_{max}, \qquad V_{max} = n \times \alpha(\Delta T_{max} + T_c)$$

Now, we need also to update the heat sink design using the newly obtained temperatures. Going back to the heat sink design of section 4.3.1. and TEC design, and substituting $T_c = 287.78\ K$ and $T_h = 312.045\ K$ gives us the new design results presented in the next chapter of the result section.

4.4 Design and Simulation of Electric Circuits of the Automatic Thermoelectric Cooling System

Electrical circuits of the automatic thermoelectric cooling system is designed using proteus software. For the simulation, Arduino software in combination with proteus software is used. The control programming is done by Arduino. As shown in Figure 4.7, the circuit diagram comprises the Arduino, DHT11 temperature and humidity sensor, fan motors, solar panel, LCD, transistor, etc.

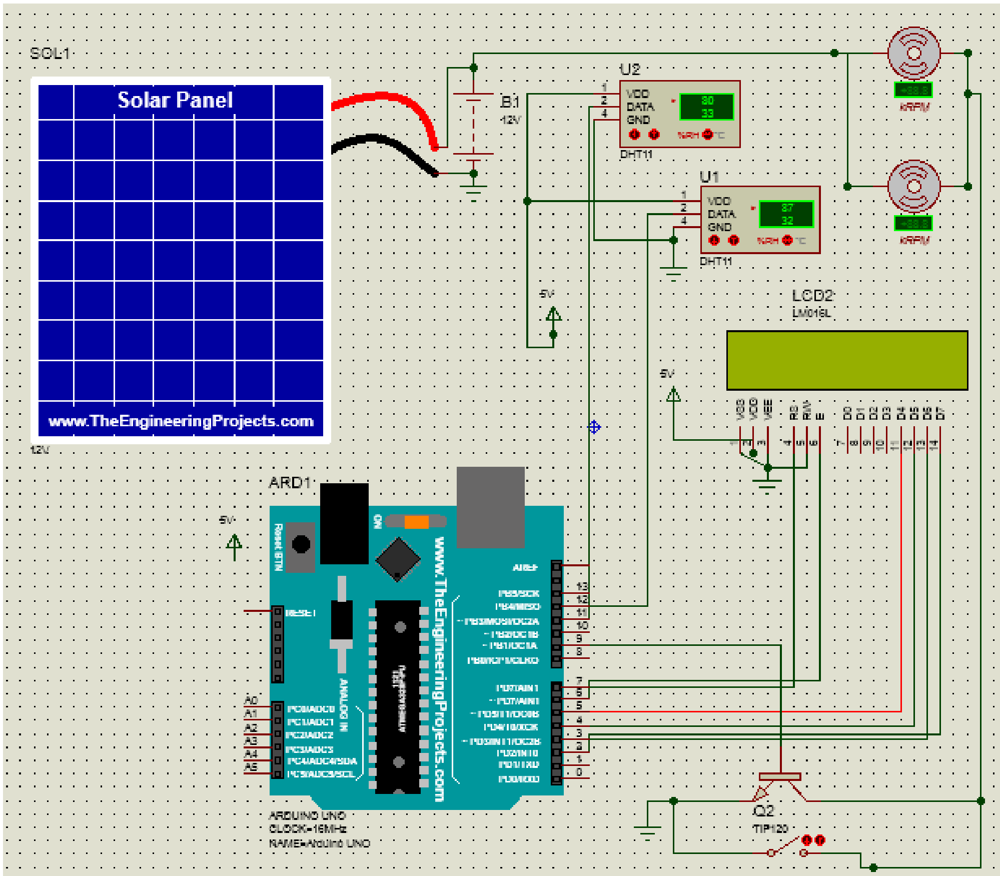

Figure 4.7: Circuit diagrams of the automatic thermoelectric cooling system

Working principles of the thermoelectric cooling system

The temperature sensor senses the cabin temperature and sends the signal to the Arduino controller. The Arduino controller then compares this value to the pre-set temperature value, which is assumed as the comfort temperature (24°C). If the temperature value from the sensor is greater than the assumed comfort temperature, the Arduino automatically turns the switch (transistor) to the TEC module and the cooling fans. Now, the cooling phase starts, the TEC module, and the cooling fans are in operation. The cooling process continues until the cabin temperature lowers down to the comfort temperature unless the driver or passenger turns the manual switch off. If the Arduino detects less or equal temperature than the pre-set temperature (24°C), it automatically turns the switch to the TEC module and the cooling fans off. Now, there is no cooling. If there is a fault on the temperature sensor and fails to sense, the cooling system will not run as it is controlled by the Arduino whose job is directly dependent on the sensor. In this case, there is a manual switch that bypasses the Arduino control. One can turn this switch to "ON" if needed to run the cooler. This cooling process continues until the passengers/driver manually switches the cooling system to "OFF". The circuit diagram simulated in Proteus is shown in Figure 4.8.

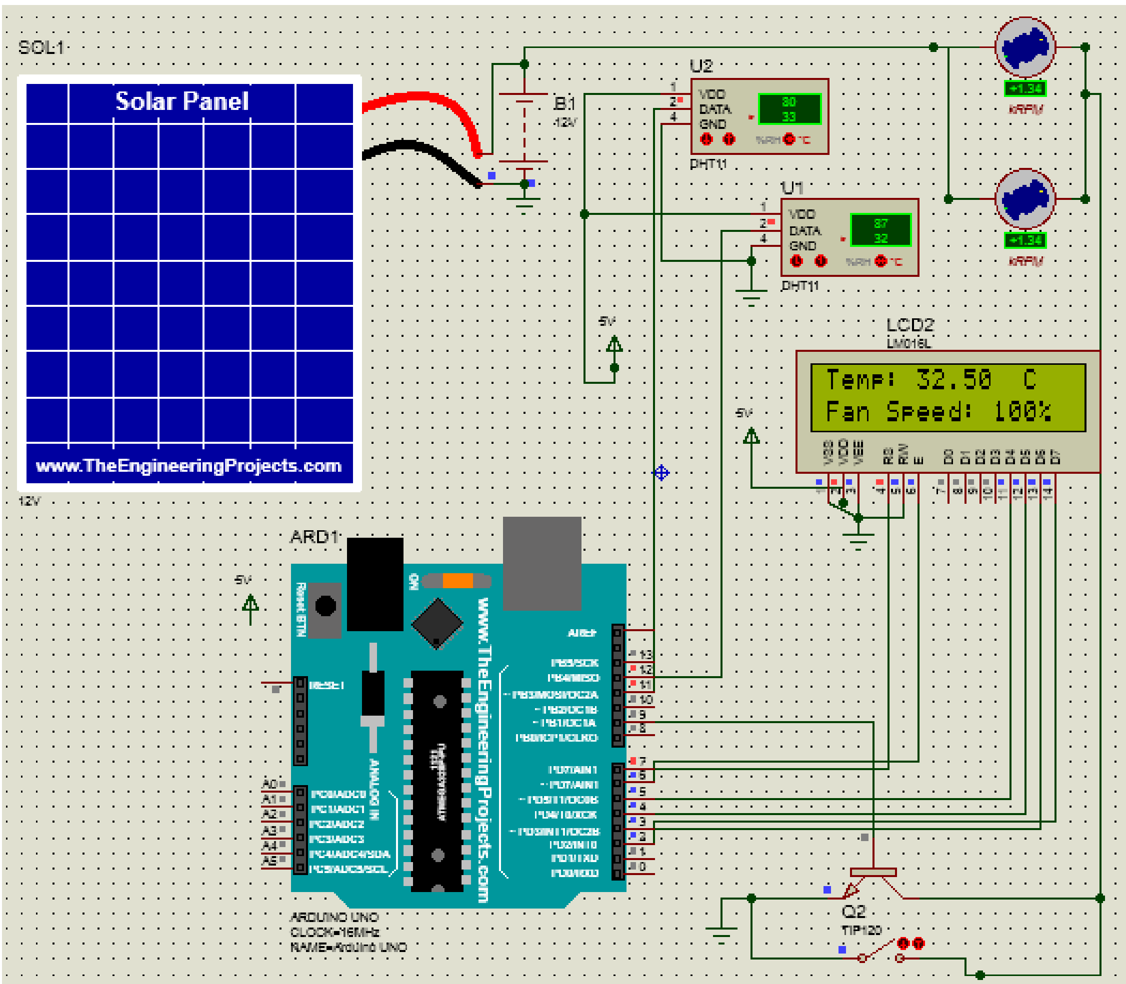

Figure 4.8: Proteus simulation diagram of the thermoelectric cooling system

(Note: TEC module isn't included in the diagram as it is not available in the proteus library. But, in the practical circuit, it is connected electrically in parallel with the cooling fans.)

4.5. Demonstration of the Automatic Thermoelectric Cooling System

The thermoelectric cooling system is demonstrated. The objective of the demonstration is to

validate whether the designed cooling system reduces the rate of the temperature increase of cabin air when parked in direct solar radiation. This can be demonstrated by recording the temperature of the cabin air and the ambient without the cooling system running and recording at another time when the cooler is running. Then comparing the temperature rise in time between the two tests the thermoelectric cooling system is validated. For the temperature measurement of both cabin and ambient air, two DHT11 sensors are used. One for the ambient and the other for the cabin. The test was held on a mid-day (at solar noon) for 3-days when maximum solar radiation is assumed to be available. For demonstration purposes, the dimensions of the following components of the cooling system are changed because of their unavailability.
Aluminum heat sinks having a dimension of 80 mm × 80 mm for internal heat sink and 90 mm × 90 mm for external are used. They have a base plate thickness of 1.9 mm; fin thickness of 1.1 mm, and fin spacing of 5.5 mm. The TEC module used for demonstration is TEC1-12706.

Cooling fans that are used for the demonstration have the following specifications.

Table 4.11: Specifications of cooling fans for demonstration

External cooling fan		Internal cooling fan	
Model:	PVA092G12H	Model:	SUNON
Dimension:	92 mm × 92 mm	Dimension:	80 mm × 80 mm
Volume low rate:	50 cfm	Volume low rate:	42 cfm

The solar panel is not used for demonstration because of the unavailability of flexible solar panels of required dimensions. Instead, a 20 W monocrystalline normal solar panel is used for running the system.

4.5.1. Manufacturing of cabin model

The car model is manufactured from aluminum sheet metal of thickness 0.8 mm and a 0.2 mm thickness of carton as insulating material. It is made with a reduction scale ratio of 1:8. After the body has got fabricated, the heat sinks and cooling fans have been installed.

Figure 4.9: Model of the car cabin fabricated from aluminum sheet metals

4.5.2. Installation of the components for the demo of the cooling system

Some of the components used for the demo of the thermoelectric cooling system are listed in Figure 4.10 below. The electrical circuit diagram with its components is shown below.

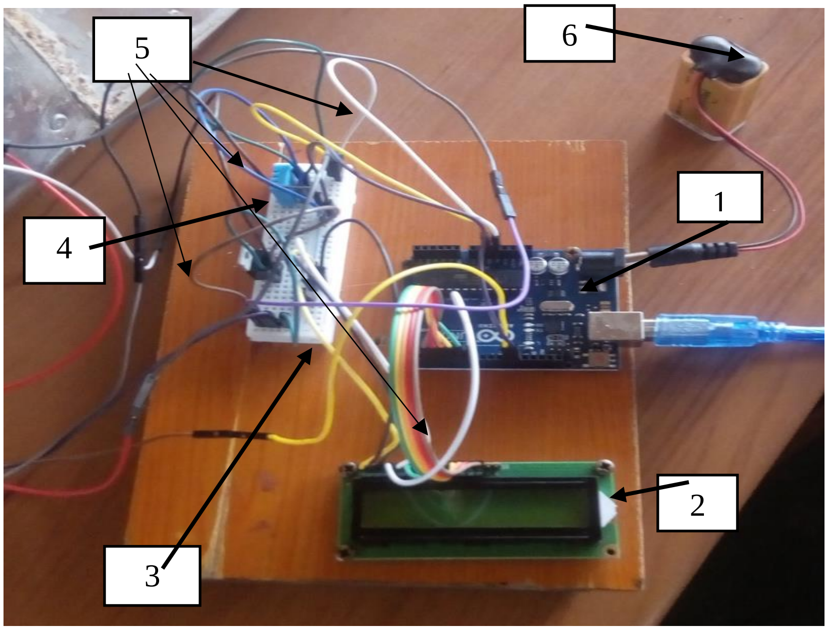

1. Arduino UNO
2. LCD
3. Breadboard
4. DHT11 temperature and humidity sensor
5. Jumper wires
6. Battery for Arduino (9 V)

Figure 4.10: Electrical control circuits of the automatic thermoelectric cooling system

As shown in Figure 4.11 the demo for the automatic thermoelectric cooling system is presented.

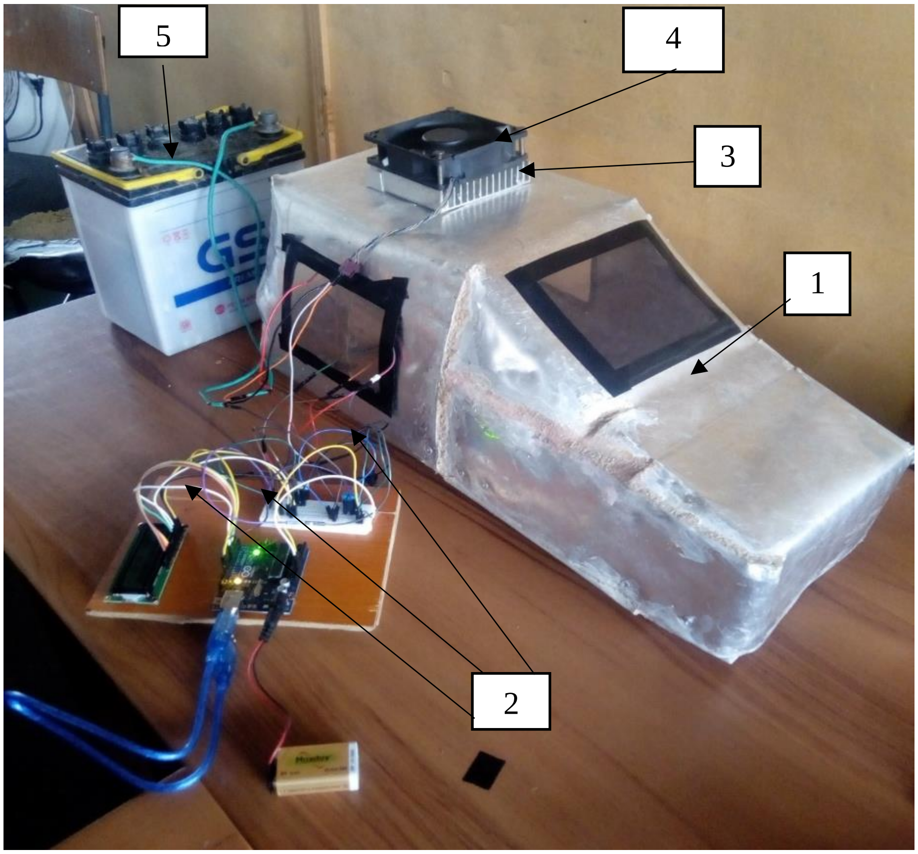

1. Car model
2. Electrical control circuit wiring
3. External aluminum heat sink
4. External cooling fan
5. Battery for fans and TEC (12 V)

Figure 4.11: The assembled demo of the automatic thermoelectric cooling system

Procedures for demonstration

1. All the components and electrical wirings were made ready for the test.
2. The car model was placed on direct sunlight and the cabin and the ambient temperatures were recorded for 44 minutes. In this case, the thermoelectric cooling system was not running.
3. Procedure number two is repeated. But, here, the cooling system was running.
4. Procedure 2 and 3 were repeated for consecutive 3 days.

Finally, the rate of the temperature rises of cabin air between when the cooling system was running and when not running is compared.

Figure 4.12: Demonstration test for the thermoelectric cooling system

4.6 Assessment of the Aerodynamic Effect of the Cooling System using ANSYS FLUENT software

To estimate the aerodynamic effects of the thermoelectric cooling system on the car, simulation result has been conducted using ANSYS FLUENT. Taking the recommended maximum driving speed of 120 km/hr into account, the simulation is performed at a vehicle speed of 120 km/hr only. Aerodynamic drag force increases with increasing vehicle speed. Therefore, the aerodynamic effect of the cooling system at a lower speed is expected to be less than that of 120 km/hr.

1. **Model description and meshing**

The Toyota Vitz 2008 car is first modeled using CATIA V5 R20 software, one with the cooling system (outside heat sinks and cooling fans) assembled to the outer roof surface of the car (Figure 4.13 (a)) and

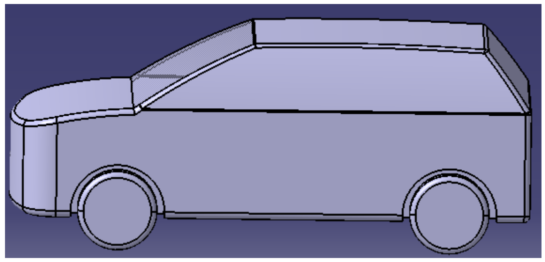

a)

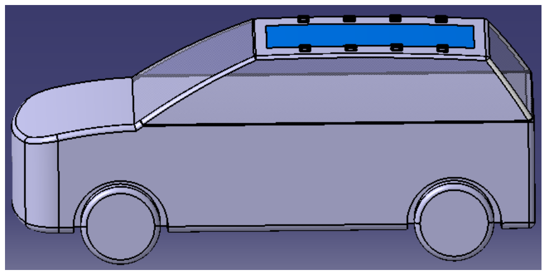

b)

Figure 4.13: 3D CATIA model of the car. (a) With no TEC cooler assembly (b) With TEC cooler assembly

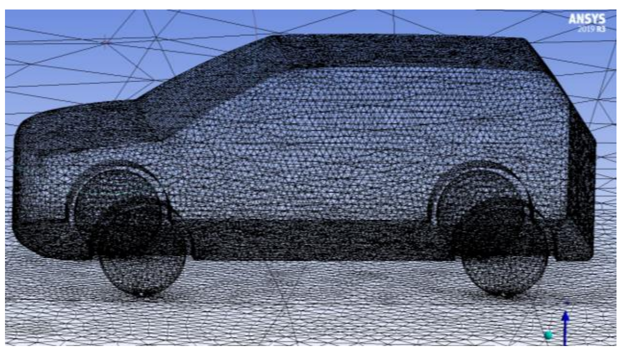

a)

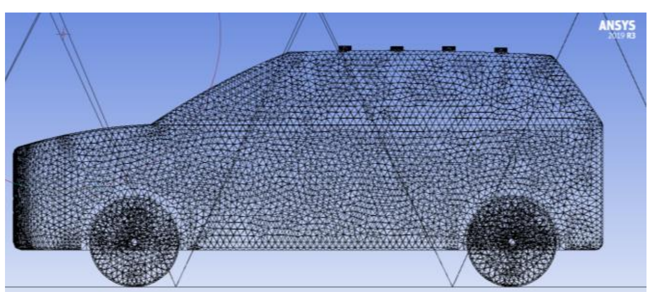

b)

Figure 4.14: Meshed view of the car a) with no thermoelectric cooler assembly b) with thermoelectric cooler assembly

the other car without the cooling system (Figure 4.13 (b)). The two-modeled cars then were imported to the ANSYS FLUENT 19.3 R3 for the aerodynamic evaluation and comparison of their drag and lift coefficient. Figure 4.14 (a) and (b) show the meshed model of the car.

2. **Setup**

Discretization is made using a second-order upwind scheme and a standard k-epsilon model was used for the simulation. A residual convergence criterion of 10^{-5} is given for the solution to converge and a hybrid solution initialization technique is used to initialize the solution.

3. **Boundary conditions**

The boundary conditions are given for the ANSYS FLUENT simulation as indicated in Table 4.12.

Table 4.12: Boundary conditions for the CFD analysis

Surface/Part	Type	Condition
Enclosure-Inlet	Velocity Inlet	Constant velocity: 33.33 m/s Turbulent intensity: 1% Viscosity ratio: 10
Enclosure-Outlet	Pressure Outlet	Gauge pressure = 0 Pa Turbulent intensity: 5% Viscosity ratio: 10
Enclosure-Sides	Symmetry	-
Enclosure-Roof	Symmetry	-
Enclosure-Floor (Road)	Walls (Moving)	Constant velocity: 33.33 m/s
Car	Walls (Stationary)	No-slip

Grid independency test

To check the dependency of the numerical results on the number of mesh elements, drag and lift coefficient simulation with various mesh elements is carried out. For the baseline car of the cooling system mesh elements 1562926, 1760523, and 2002888 are simulated. While, for the car with the cooling system, simulations with mesh elements of 1428333, 2218611, and 2545739 are done.

CHAPTER FIVE

RESULTS AND DISCUSSIONS

In this chapter, results obtained from the design of the automatic thermoelectric cooling system are listed and briefly explained. Design results of internal heat sinks, thermoelectric module, and results of drag and lift coefficients of the car are well enumerated and discussed. How the automatic thermoelectric cooling system works is also demonstrated.

5.1. Thermoelectric Cooling System

Results obtained from the analytical design of the TEC module and the aluminum heat sinks are presented and discussed as follows.

5.1.1. Heat sinks

Heat sinks design with cooling fans at both sides, with cooling fans at internal sides only, and with cooling fans at external sides only, are considered. Their results are listed as follows:

5.1.1.1. Heat sinks with cooling fans at both sides

Figures (5.1) (a) and (b) demonstrate that as the thickness of the fins of aluminum heat sinks decreases, the heat dissipation rate of the heat sink is increased up to some point of the thickness of fins. It then decreases with decreasing the fin thickness. The rate of heat absorption/dissipation through fins of aluminum heat sinks decreases asymptotically with the increase in fin thickness. The optimum fin thickness of the internal heat sinks for the maximum rate of heat absorption is 0.058 mm. For the external heat sink, the optimum fin thickness for the maximum rate of heat dissipation from the TEC to the ambient is 0.06 mm.

The maximum rate of heat absorption/dissipation through internal and external heat sinks is 53.14W and 160.95 W respectively. The cooling capacity of the heat sinks is high when installed with forced convection.

(Note: All graphs for the rate of heat dissipation versus fin thickness for the aluminum heat sinks are taken from Mathcad prime 7 software. Subscripts 1 and 2 represents internal and external heat sink respectively)

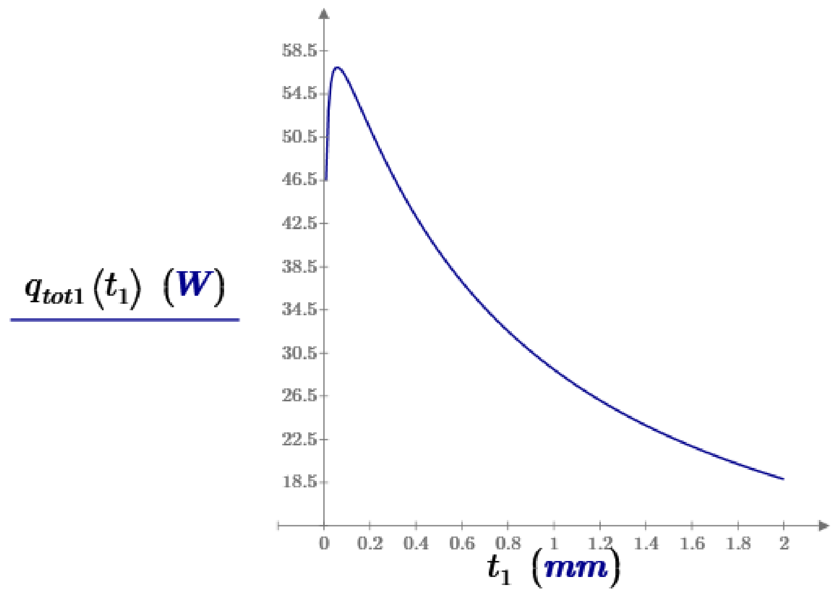

(a)

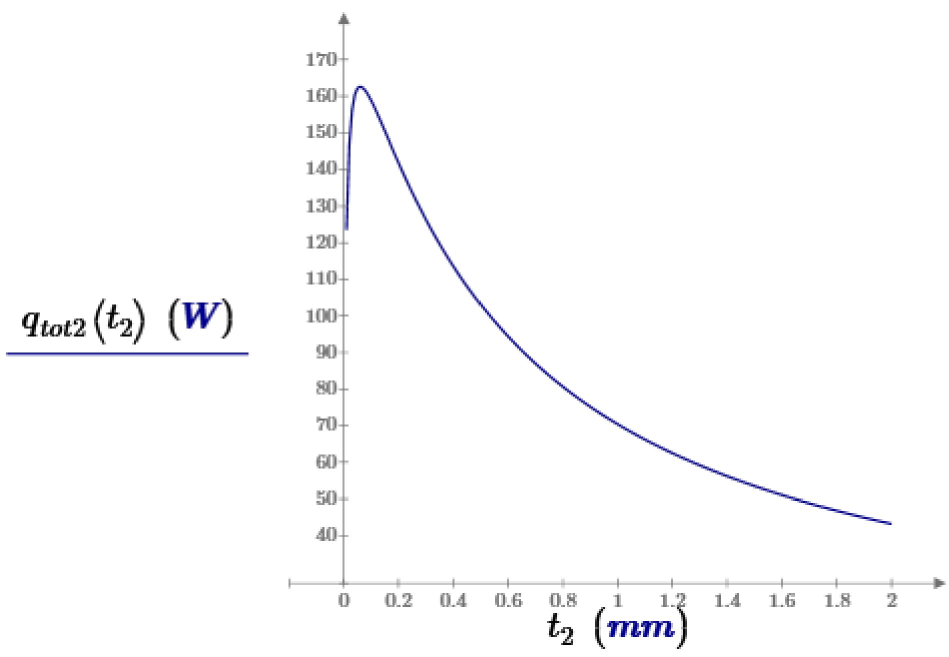

(b)

Figure 5.1: Total heat transfer rate versus fin thickness (by Mathcad software) (a) internal aluminum heat sink (b) external aluminum heat sink

5.1.1.2. Heat sinks with free convection at both sides

Figure 5.2 (a) and (b) indicate the rate of heat dissipation through heat sink versus fin thickness.

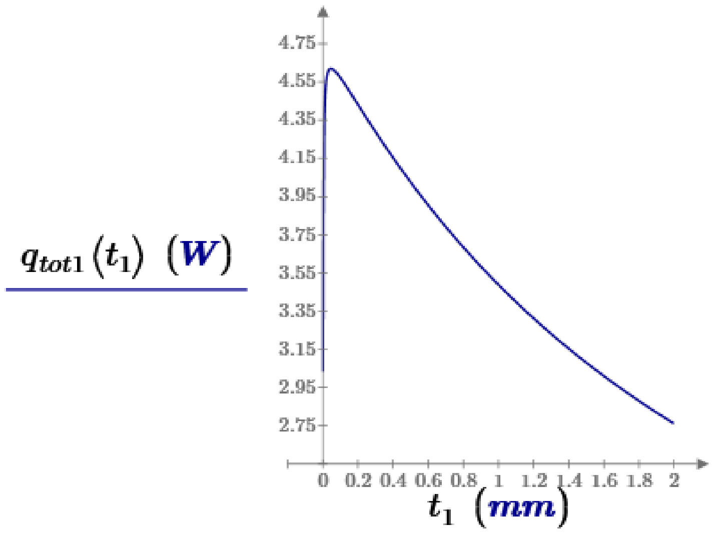

(a)

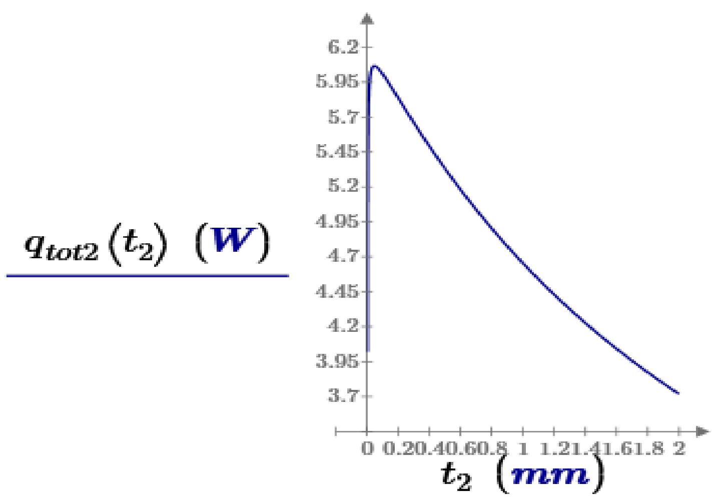

(b)

Figure 5.2: Total heat transfer rate versus fin thickness (a) internal aluminum heat sink (b) external aluminum heat sink

Figure (5.2) (a) and (b) shows the indirect proportionality of the thickness of the fins and the heat dissipation rate of the heat sinks. For natural convection heat sinks, the rate of heat dissipation is about 4.6 W for internal heat sinks and about 6.0 W for external heat sinks. These are much less than that of forced convection heat sinks. Generally, aluminum heat sinks of the specified dimensions are not effective for absorbing/dissipating a larger heat load for the thermoelectric cooling system.

The optimum fin thickness of the internal heat sinks for the maximum rate of heat absorption is 0.046 mm. For the external heat sink, the optimum fin thickness for the maximum rate of heat dissipation from the TEC to the ambient is 0.05 mm.

5.1.1.3. Heat sinks with free convection at the internal side and forced convection at the external side

In the same manner as Figure (5.2), the rate of heat transfer for the internal side is very low due to free convection heat sinks (Figure 5.3 (a)). On the other hand, the rate of heat transfer on the outside (external) aluminum heat sinks is high because of the forced convection due to the outer cooling fans (Figure 5.3 (b)).

Although the external heat sinks are enough to dissipate the heat coming from the cabin air, due to the very low heat transfer rate at the internal heat sinks, the overall cooling effect is decided by the internal heat sinks. Because the cooling effect depends on both the internal and external aluminum heat sinks. Therefore, the maximum cooling capacity of the thermoelectric cooling system (with free convection at the internal side and forced convection at the external side) is less than 4.7 W.

The optimum fin thickness of the internal heat sinks for the maximum rate of heat absorption is 0.217 mm. For the external heat sink, the optimum fin thickness for the maximum rate of heat dissipation from the TEC to the ambient is 0.2 mm.

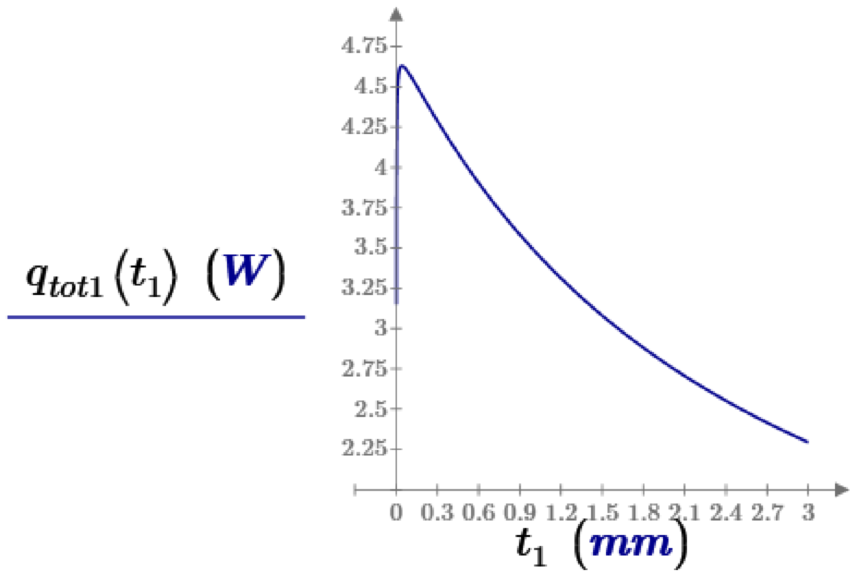

(a)

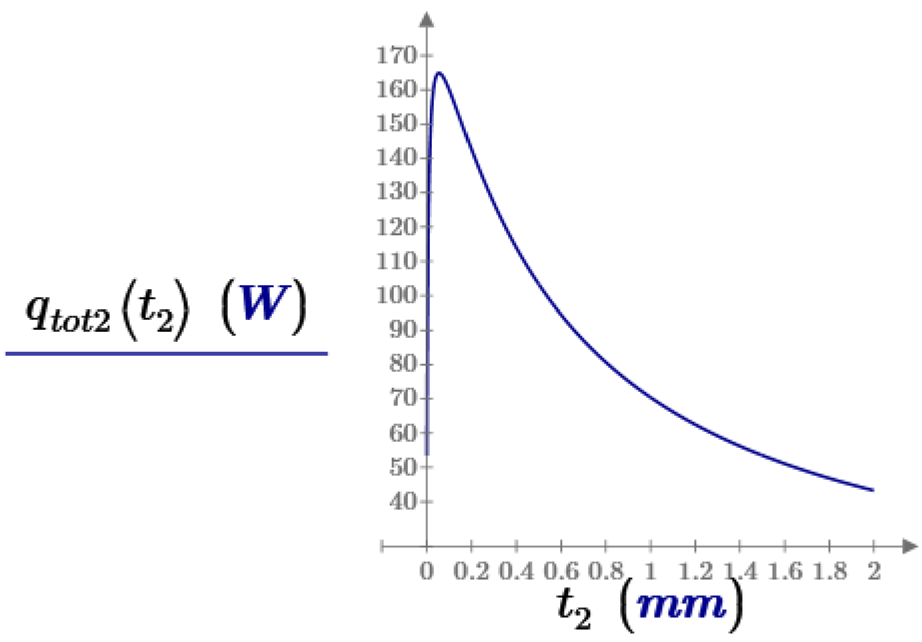

(b)

Figure 5.3: Heat transfer rate versus fin thickness. (a) Internal aluminum heat sink. (b) External aluminum heat sink.

When comparing Figures (5.1), (5.2), and (5.3) for their heat absorption/dissipation rate, heat sinks with cooling fans at both sides (internal and external) have a maximum cooling capacity of 53.14 W and 160.95 W. The heat absorption/dissipation rate through the rest of the design results is low. Therefore, aluminum heat sinks with forced convection at both sides are taken best for the thermoelectric cooling system. As a result, the cooling capacity of the designed thermoelectric cooling system is estimated taking this consideration into account.

5.1.2. TEC module

TEC module is designed based on maximum cooling capacity, maximum coefficient of performance, and the mid-point between the design on the maximum cooling capacity and the design based on the maximum coefficient of performance. Results obtained from the three-basis design are listed and discussed. Cooling capacity and input electrical power versus temperature gradient, coefficient of performance versus input electrical current, cooing capacity versus input electrical current are graphically presented and discussed.

5.1.2.1. TEC based on the maximum cooling capacity

According to these design criteria, the aim is to have maximum cooling capacity. Based on this design the temperature gradient is taken as 35℃. The current for the maximum cooling power is calculated as 7.36 A. Figure (5.4) shows that at this ΔT, the maximum cooling power is about 36.49 W. However, the input electrical power increased to about 116.33 W. This indicates that based on the design, there is a high demand for electrical power. The design has a very low coefficient of performance of 0.3 (Figure 5.5).

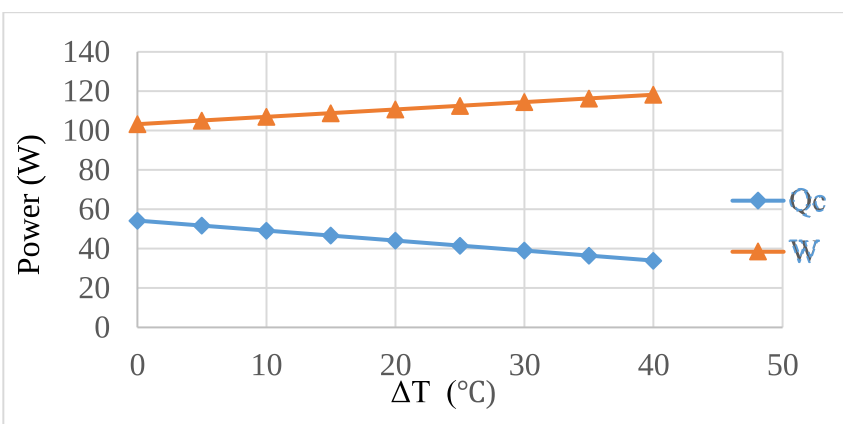

Figure 5.4: Cooling capacity and input electrical power versus the temperature gradient between the hot and cold sides of TEC module

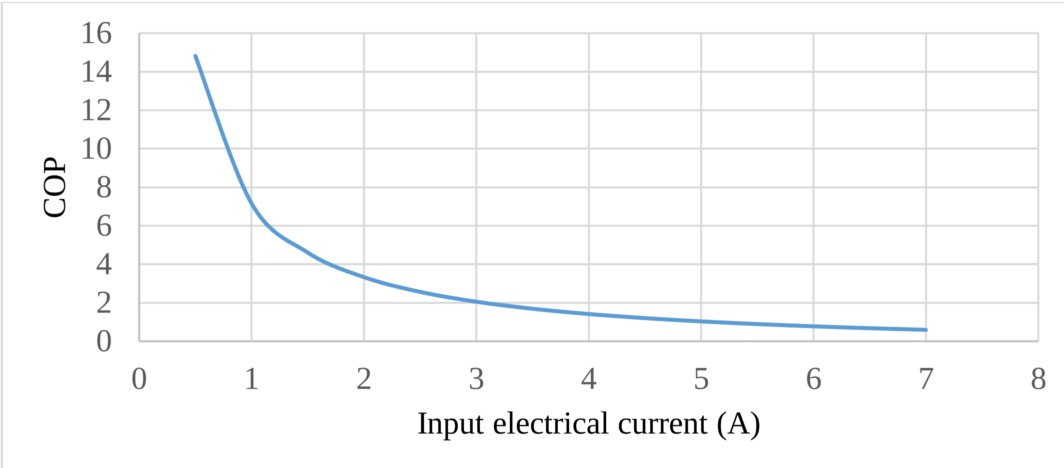

Figure 5.5: Coefficient of performance versus input electrical current for TEC module

5.1.2.2. TEC based on the maximum coefficient of performance

This design is aimed at saving electrical input power. The optimum electrical current for the maximum coefficient of performance at a temperature gradient of 35℃ is obtained as 2.75 A. As shown in Figure (5.6), the cooling capacity at this ΔT is 14.65 W. The input electrical power required at this temperature gradient is 19.4 W (look at Figure 5.7 below). At the indicated electrical input current it has a COP of 0.75 (look at Figure 5.8). Although this design demands low input power, it has a low cooling capacity.

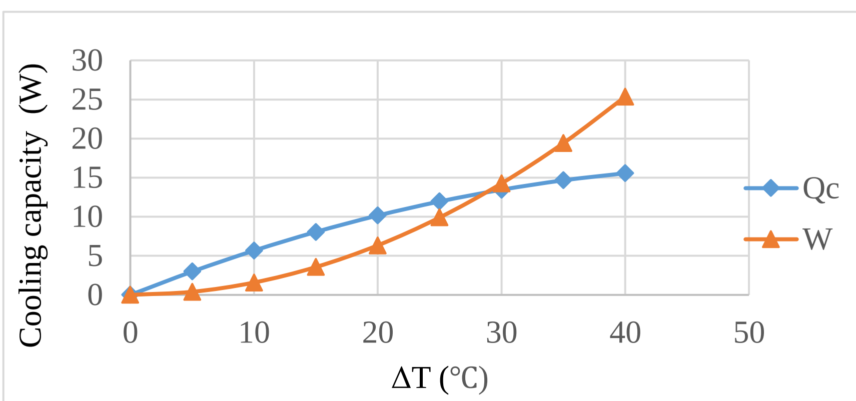

Figure 5.6: Cooling capacity and input electrical power versus the temperature gradient between the hot and cold sides of TEC module

In Figure (5.6) the cooling capacity increases with increasing the temperature gradient. It is because the required input electrical current for the maximum coefficient of performance is directly proportional to the temperature difference between the cold and hot sides of the module. As ΔT increases, the demand for input electrical current also increases. The increase in electrical input current directly means the increase in the cooling capacity. To summarize, for the maximum coefficient of performance of the TEC module the current cooling capacity increases with increasing the temperature gradient between the cold and hot junctions.

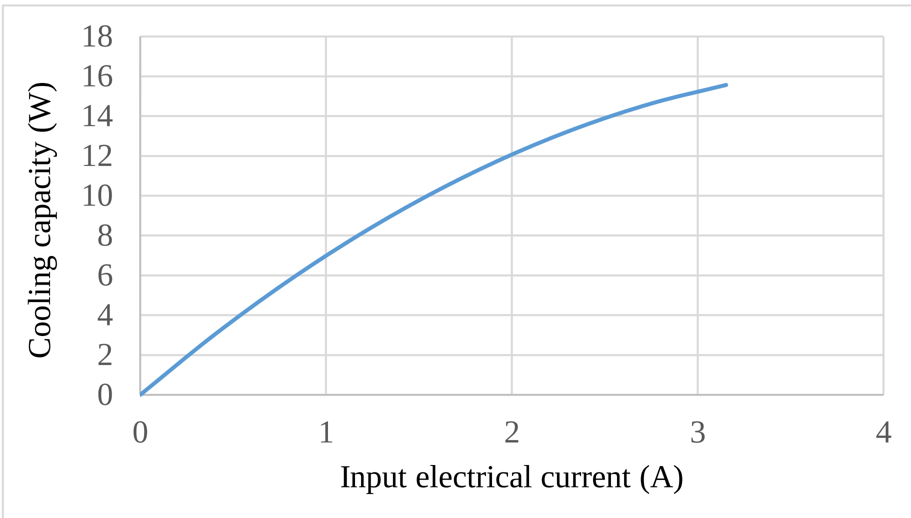

Figure 5.7: Cooling capacity versus electrical current for TEC module

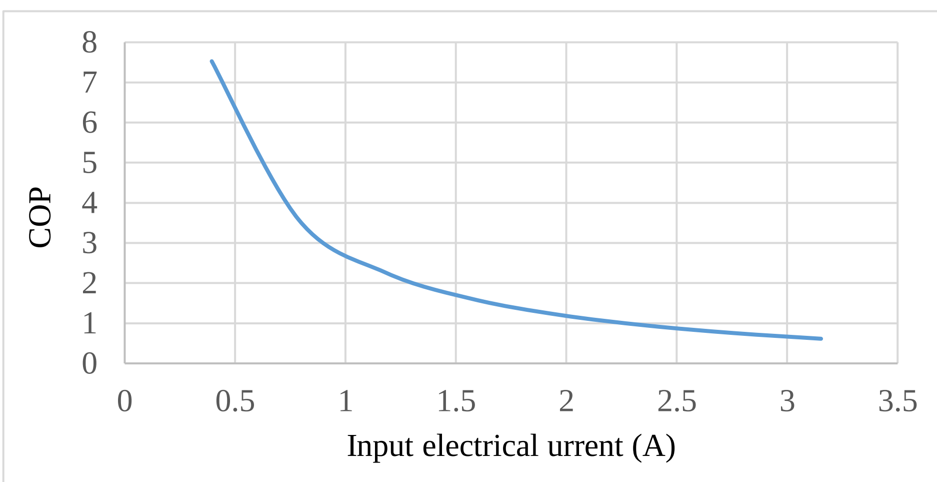

Figure 5.8: Coefficient of performance versus input electrical current for TEC module

5.1.2.3. TEC module based on the midpoint of the current between maximum cooling power and maximum coefficient of performance

This design is optimized for the cooling power and the COP. The optimum midpoint input electrical current at the design temperature is obtained as 5.06 A. The optimum cooling capacity obtained at this optimum input current is 30.61 W (Figure 5.9 @$\Delta T = 35$ °C). As shown in Figure (5.9) the power required to get this cooling capacity is 57.78 W. The coefficient of performance is 0.52 (Figure 5.10 at I = 0.52 A).

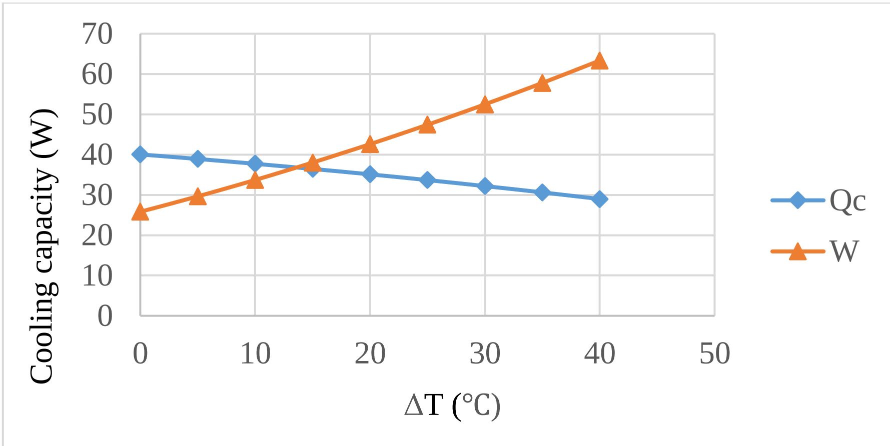

Figure 5.9: Cooling capacity and input electrical power versus the temperature gradient between the hot and cold sides of TEC module

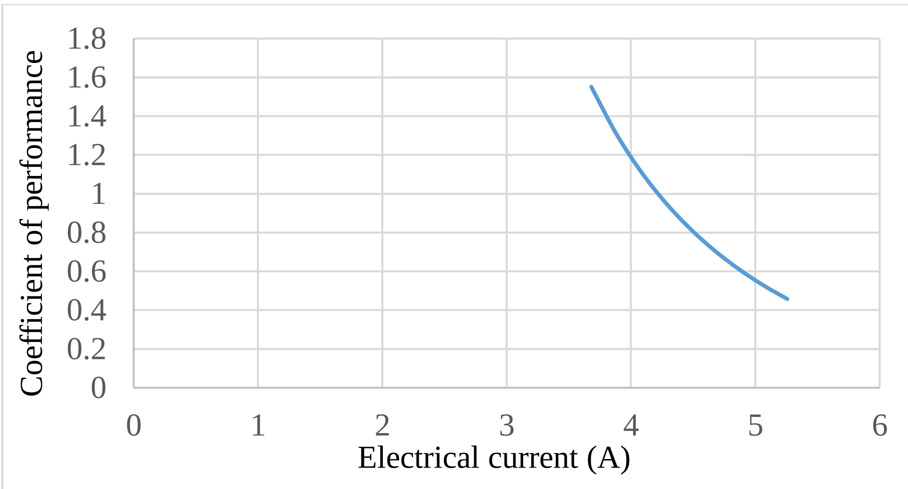

Figure 5.10: Coefficient of performance versus input electrical current for TEC module

5.1.3. Design Summary

For automotive applications of thermoelectric cooling, both maximum cooling power and COP are needed. In this thermoelectric cooling system, as the power source is a solar panel, the power usage by the thermoelectric cooling system should be as low as possible. However, a high cooling capacity is needed to cool the cabin air within a small period. Therefore, to compromise the two needs, the mid-point design is selected. It has been adjusted that the power for the TEC is based on a 12 V power source.

The cold side and hot side temperatures are updated so that the heat sinks and TEC go in line with each other. It is obtained that Tc = 287.78 K and T_h = 312.045 K. After substituting the updated values of T_c and T_h, the following results are obtained for the heat sinks and thermoelectric cooler. Figure (5.12) shows the results of the heat sink design after the cold and hot side junction temperatures are updated.

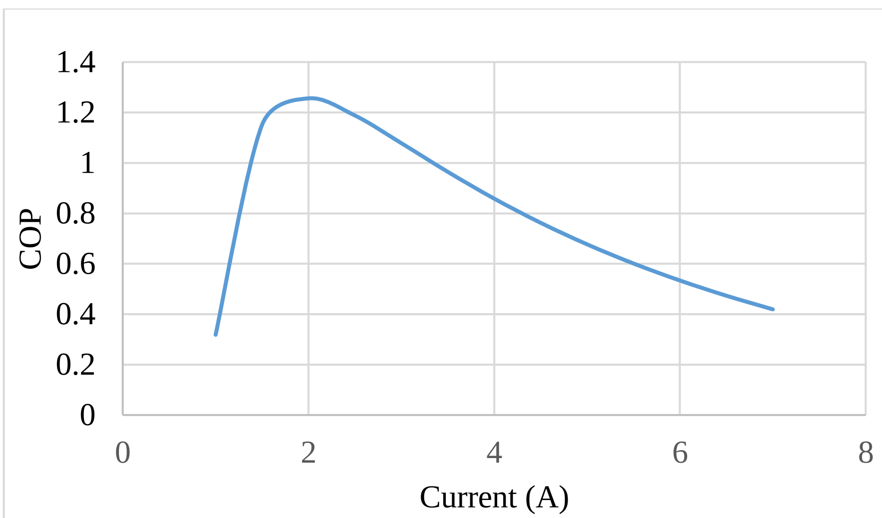

Figure 5.11: Coefficient of performance of TEC module with input electrical current

From Figure (5.11), we see that the coefficient of performance of the TEC module initially increases and later declines. This is due to as we increase the electrical current to the module, the joule heat increases. The maximum COP is registered at an input current of 2 amperes.

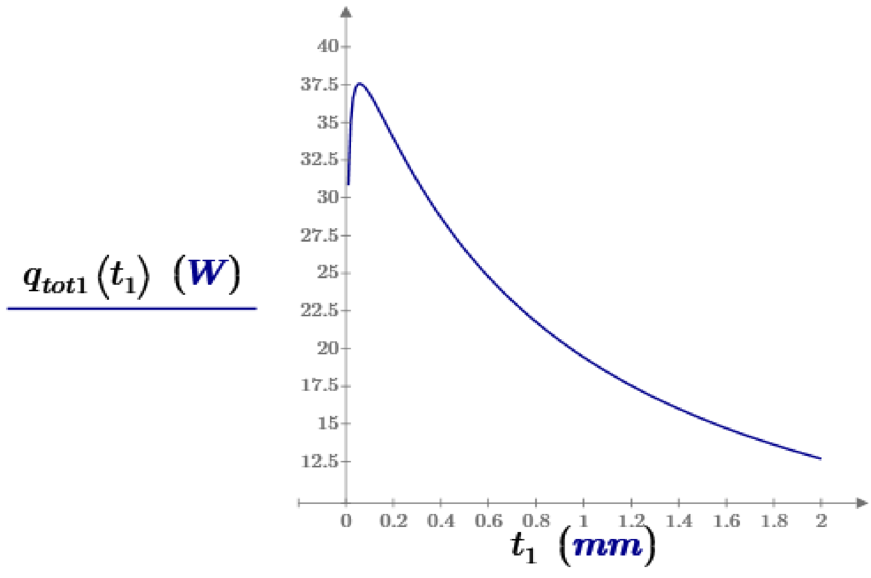

(a)

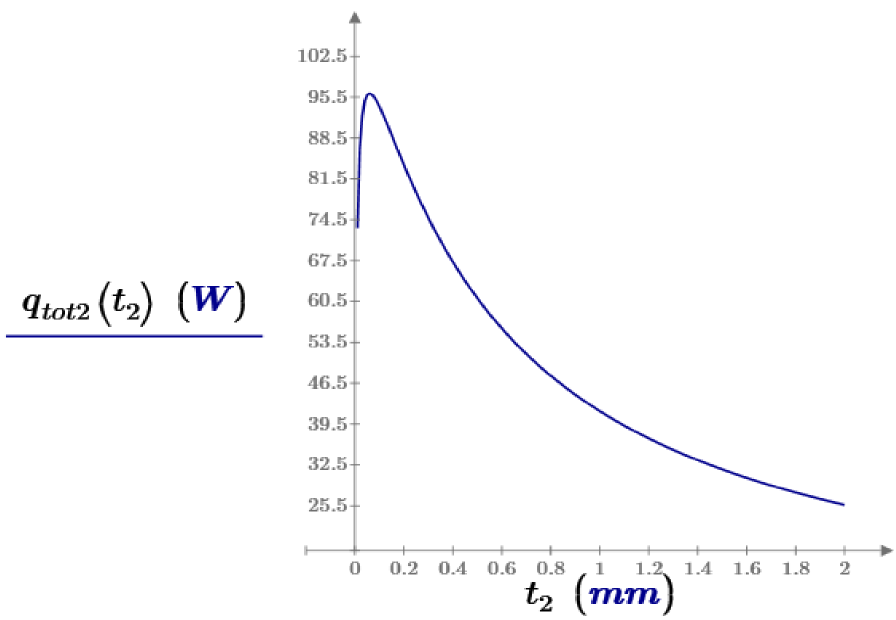

(b)

Figure 5.12: Heat dissipation rate versus fin thickness (a) internal heat sink (b) external heat sink

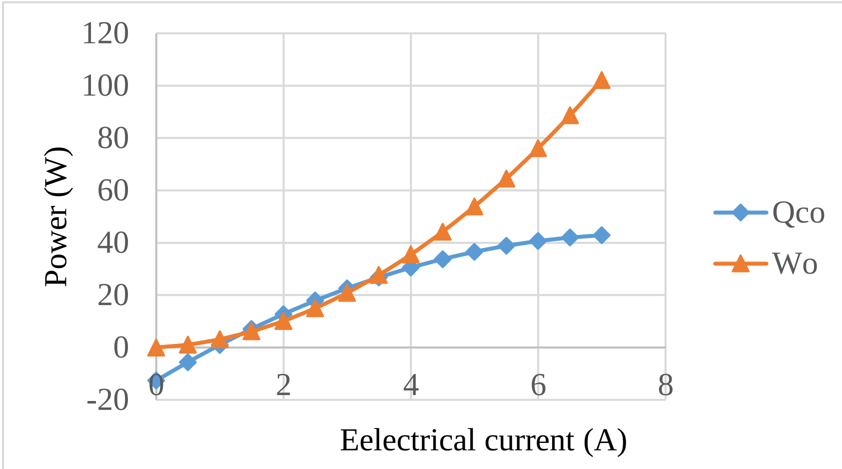

Figure 5.13: Cooling capacity of TEC module with input electrical current

As we see from Figure (5.13), the cooling capacity of the TEC module increases with the increasing input electrical current

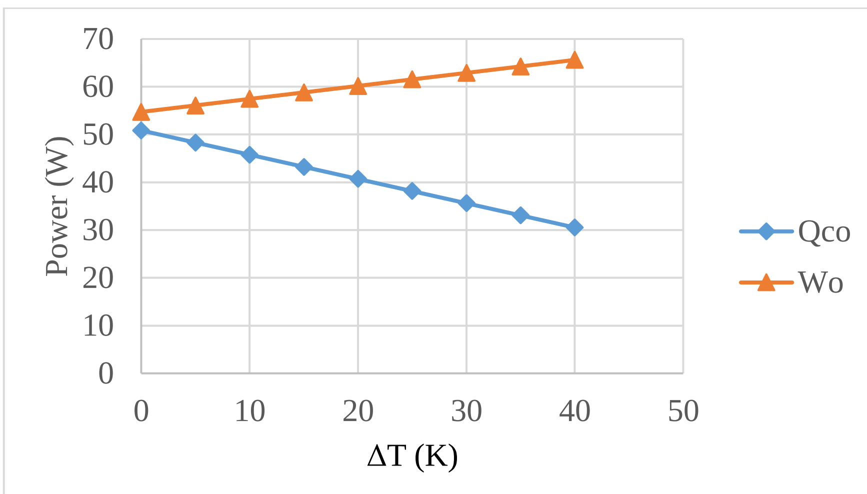

Figure 5.14: Optimum cooling capacity of TEC with ΔT between the hot and cold sides of TEC module

The heat transfer rate depends on the temperature gradient. However, here, the temperature gradient, in this case, is the difference between the cold and hot junction temperatures of the TEC module. As the temperature gradient increases, there is a heat transfer from the hot side to the cold side of the TEC module. The cold side of the module will gain some amount of heat from the hot side of the module via the thermocouples and ceramic plates. This inhibits the cooling capacity of the TEC module. Generally, as it is seen from Figure (5.14) the cooling capacity of the TEC module decreases with the increase in the temperature gradient.

From the design results of heat sinks and TEC modules, it can be concluded that the heat sinks and TEC modules are compatible. Therefore, the cooling capacity and performance of the thermoelectric cooling system are estimated in the next section.

Table 5.1: The final over all result summary of the heat sinks and TEC module

Heat sink			TEC	
Parameters	Internal	External	Parameters	Optimum
Heat loads (W)	38.142	96.41	Cooling rate (W)	38.08
Fin thickness (mm)	0.058	0.06	Input power (W)	58.59
Fin spacing (mm)	0.8	0.54	Heat rejected (W)	96.67
Number of fins	84	134	COP	0.65
Mass of fins (gm)	5	9	Voltage (V)	12
Overall efficiency	0.93	0.89	Current (A)	5.23
Overall thermal resistance (m^2K/W)	0.246	0.092	Q_{cmax} (W)	52.94
Length (mm)	70	80	ΔT_{max} (K)	108.56
Width (mm)	70	80	V_{max} (V)	20.10
Height (mm)	5	5	I_{max} (A)	7.66

The minimum fin thickness to manufacture is 0.11 mm (https://www.dhtnet.com/products/). Taking this consideration into account, the fin thickness of internal and external heat sinks is taken as 0.15 mm and 0.2 mm respectively. At this fin thickness, the maximum heat dissipation rate through the internal and external aluminum heat sinks is 35.92 W and 84.14 W respectively. Therefore, the cooling capacity of the thermoelectric cooling system is limited to 35.92 W.

5.2. Cooling Capacity of the Thermoelectric Cooling System

The maximum number of sunshine hours per day is 5 hrs. The total power the solar panel could generate per day is 875 W. If the minimum sunshine hour is 4 hours per day; it can generate 700 W per day.

Solar Panel power output = 95% of its rated power.

Solar charge controller efficiency = 98%

Battery efficiency = 85% (lead acid battery)

The minimum usable electric power P from the battery is:

$$P = P_{SP} \times \eta_{SP} \times \eta_{Ch} \times \eta_{b} \tag{5.1}$$

Where,

P_{SP} is the power produced by the solar panel,

η_{SP} is the efficiency of the solar panel,

η_{Ch} is the efficiency of the solar charge controller,

η_{b} is the efficiency of the battery.

From equation (5.1), the minimum and maximum daily power obtained from the battery is 554 W and 692 W respectively. If we take the average, it is 623 W. Therefore, for the complete thermoelectric cooler assembly, the daily power usage is limited to 623 W.

From the design result, the optimum cooling capacity of a TEC module at ΔT of 24.865 K and input electrical current of 5.23 A is 38.24 W. But, the internal heat sink with the specified fin thickness can only absorb about 35.92 W. The optimum coefficient of performance of TEC is 0.65. That means the input electrical power required for a single TEC module is found to be 55.26 W. The internal and external cooling fans used have a power rating of 1.74 W and 4.3 W respectively.

The power required to run a TEC module installed with both internal and external heat sinks and cooling fans is 61.30 W. The number of TEC modules with two cooling fans (one internal and one external) we could have for the thermoelectric cooling system is determined as follows:

From the solar panel, an average power of 623 W per day is produced. The efficiency of the heat sinks is 0.93 for internal and 0.89 for external.

The total rate of heat dissipation Q_c from the car cabin by the thermoelectric cooling system is

$$Q_c = 35.92 \times 0.93 \times 8 = 267.24 \text{ W}.$$

This is 31.01% of the total rate of heat gain by the parked car cabin having no occupants from different heat sources and the surrounding.

5.3. Simulation of the Effect of Thermoelectric Cooling System on the Aerodynamics of the Car

Aerodynamic drag and lift coefficients along with their corresponding forces are simulated in ANSYS FLUENT. The simulation is conducted for both the baseline car and the car with the thermoelectric cooling system assembly. The result obtained is presented in the following section.

5.3.1. Aerodynamic coefficients of the car free of the cooling system

Table (5.2) lists the aerodynamic lift and drag coefficients and the corresponding forces simulated in ANSYS FLUENT 19.3.

Table 5.2: Aerodynamic drag and lift coefficients for the baseline car

Mesh elements	Drag coefficient	Lift coefficient	Drag force (N)	Lift force (N)
1,562,926	0.278	-0.006	-432.65	-9.336
1,760,523	0.273	-0.001	-424.868	-2.489
2,002,888	0.286	-0.062	-445.100	-96.470

The deviation in percent of the drag coefficients for Table 5.2 between mesh elements of 1562926 and 1760523 is 1.8% and of between 1760523 and 2002888 is 4.76%. Therefore, the drag coefficient of less deviation and the fine mesh is taken. I.e., Cd = 0.273 for the car with no thermoelectric cooling system.

As shown in Figure 5.15 (a) the result of the drag coefficient simulated in ANSYS 19 R3 is 0.273. The result of the aerodynamic lift coefficient before the installation of the thermoelectric cooling system is -0.0016 (Figure 5.15 (b)).

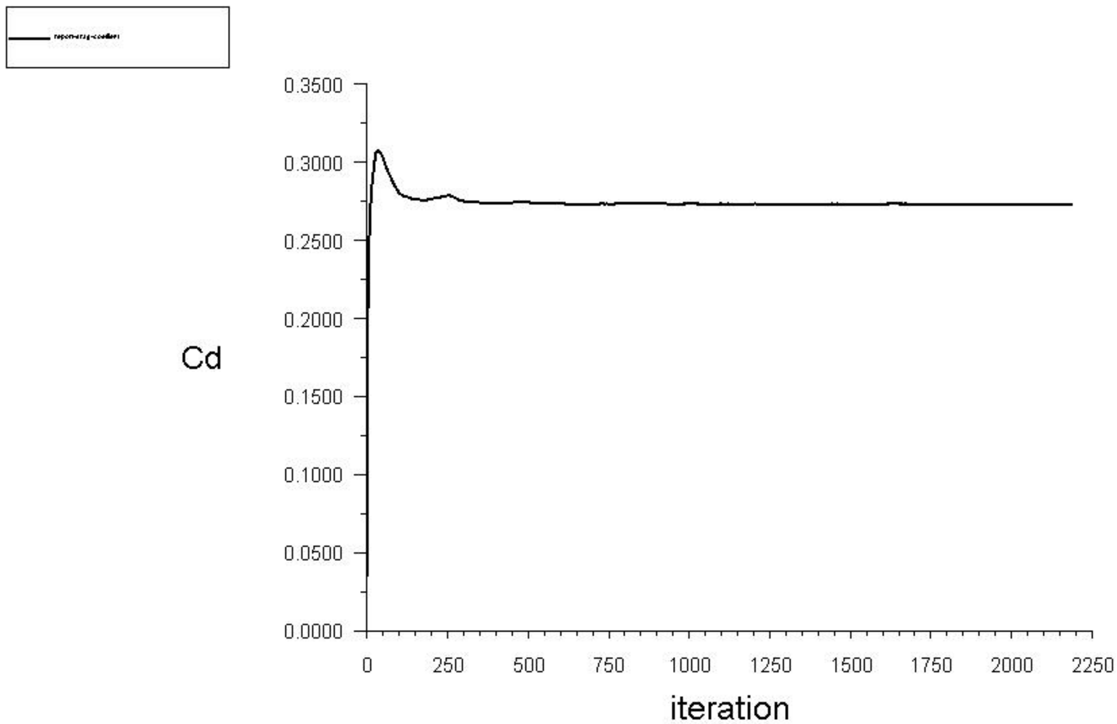

(a)

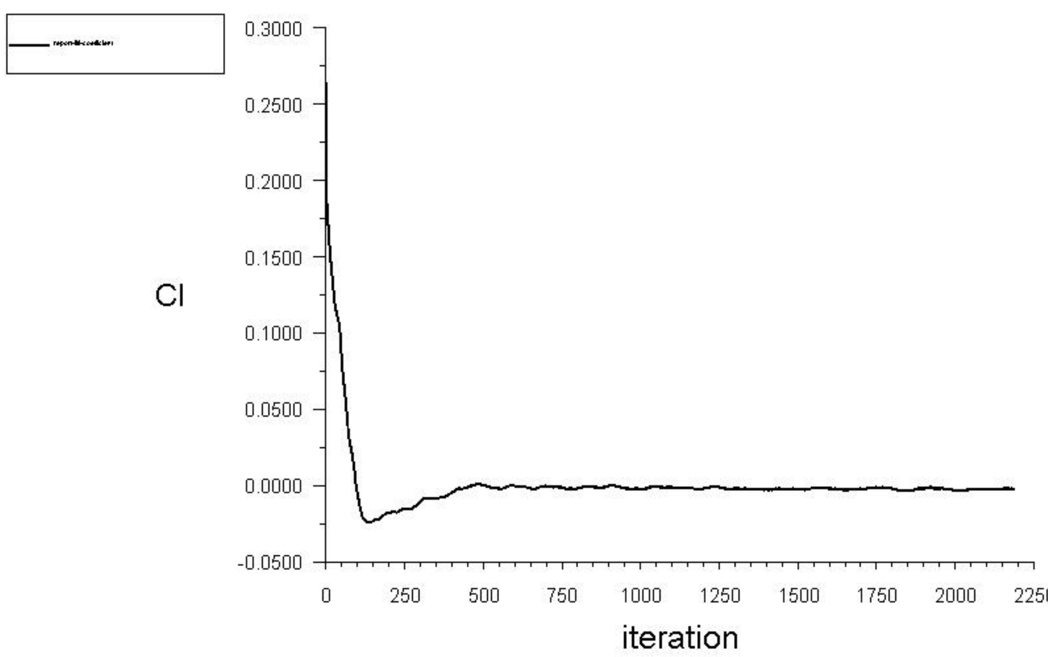

(b)

Figure 5.15: Aerodynamic coefficients of the baseline car. (a) Drag coefficient. (b) Lift coefficient

5.3.2. Aerodynamic coefficients of the car with the thermoelectric cooling system

Figure 5.16 (a) and (b) show the drag and lift coefficients as follows.

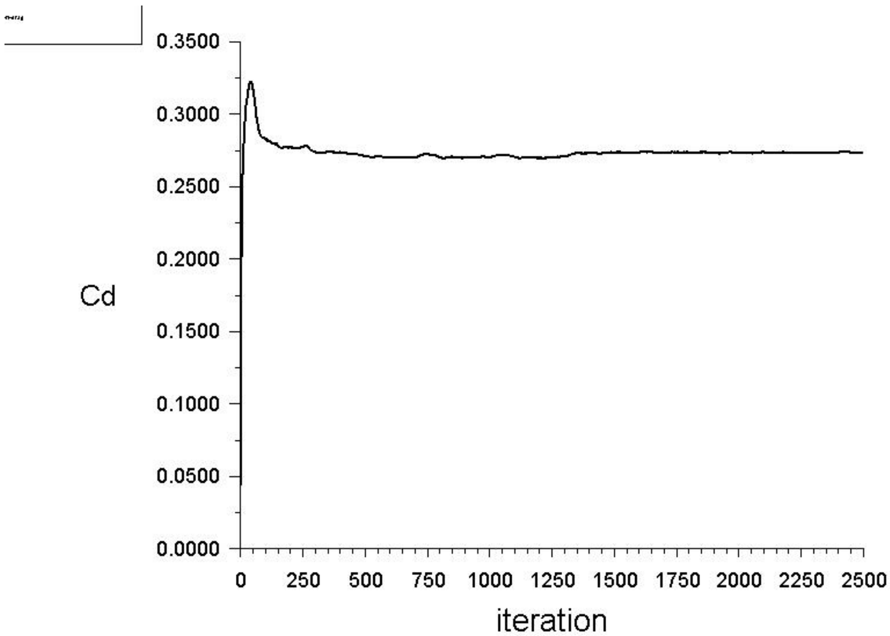

(a)

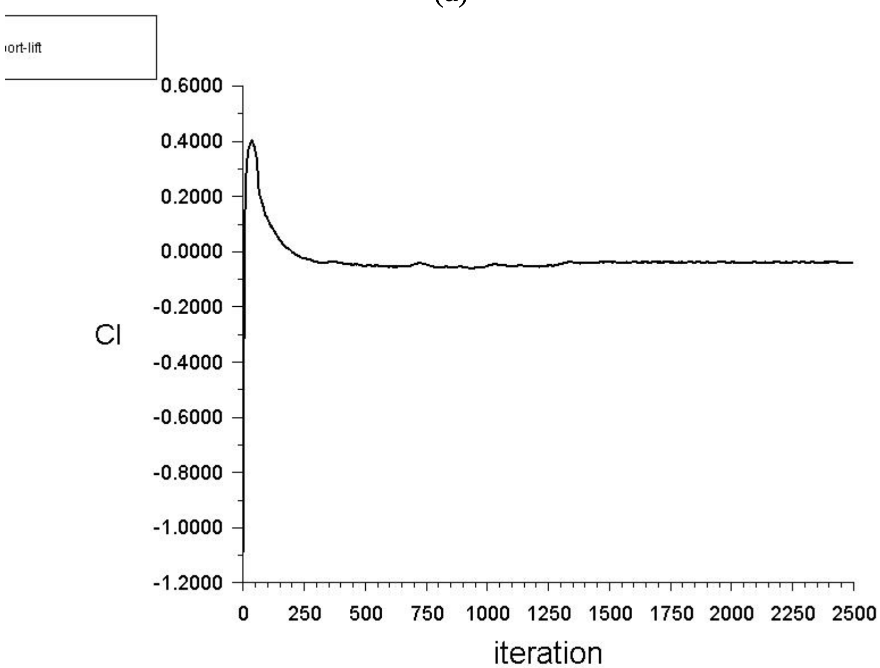

(b)

Figure 5.16: Aerodynamic coefficient of the car with the thermoelectric cooling system. (a) Drag coefficient (b) lift coefficient

Table 5.3: Aerodynamic drag and lift coefficients for the car with the cooling system

Mesh elements	Drag coefficient	Lift coefficient	Drag force (N)	Lift force (N)
1,428333	0.304	-0.004	-473.680	-6.232
2,218,611	0.275	-0.037	-428.494	-58.430
2,545739	0.315	-0.030	-490.820	-46.740

Following the same evaluation as Table (5.2) for Table (5.3), the drag coefficient of the car with the thermoelectric cooling system is 0.275.

The aerodynamic drag after the cooling system has been installed in the car is 0.275 as shown in Figure 5.16 (a). The aerodynamic lift coefficient of the car after the cooling system installation is -0.0375 (Figure 5.16 (b)).

Resistance power added

Resistance power added on the car due to the installations of the thermoelectric cooling system with respect to the car with no thermoelectric cooling system is calculated using the equation given below (Kim, 2011).

$$P_{added} = (F_2 - F_1) \times V_{car} \tag{5.2}$$

Where,

P_{added} = Additional power required due to the increase in aerodynamic drag (W)

F_2 = Drag force of the car with the thermoelectric cooling system (N)

F_1 = Drag force of the car with no thermoelectric cooling system (N)

V_{car} = Speed of the car (m/s)

Substituting the values of the drag forces selected from Table (5.2) and (5.3), and taking speed as 33.33m/s gives:

$$P_{added} = 120.85 \text{ W}.$$

Additional Fuel required due to the thermoelectric cooling system

Fuel added by the increase of the drag force is calculated using the equation given below (Kim, 2011).

$$\dot{m}_{fuel} = \frac{P_{added}}{Q_{LHV} \times \rho_{fuel} \times \eta_{engine}} \tag{5.3}$$

Where,

$\dot{m}_{fuel}$ = Mass flow rate (m^3/s)

P_{added} = Power added (W)

Q_{LHV} = Lower heating value (lower heating value of diesel fuel is 42.5 MJ/kg)

ρ_{fuel} = Density of fuel at ambient temperature (860 kg/m^3)

η_{engine} = Thermal efficiency of the engine (thermal efficiency of the engine is 35%)

Substituting the given values in equation (5.3) results: $\dot{m}_{fuel} = 1.038 \times 10^{-8}\ m^3/s$ = 0.037 L/hr.

5.4. Validation of the Designed Results

The maximum plate-fin efficiency is 1. The overall fin efficiency obtained in this design is below 1. So it is acceptable.

The COP of a single-stage thermoelectric cooler module is between 0.3 and 0.7 (https://thermalbook.wordpress.com/cop-of-a-thermoelectric-cooler-tec/). The COP result obtained in this design is 0.65. Therefore, it is acceptable.

The cooling capacity of a TEC module varies depending on the semi-conductor materials made of, the number of thermoelements used, the temperature gradient between the cold and hot sides of the module, and the amount of input electrical power used. TEC modules in the market (TEC12705) resembling the designed TEC module has a maximum cooling capacity of 43.49 W (look at the datasheets of TEC12705). The maximum cooling capacity of the designed TEC in this study is 52.94 W. Both the designed TEC and TEC1-12705 are made of 127 thermocouples. The maximum input current for both of these modules is nearly the same. 5.23 A for the TEC designed in this paper and 5.3 A for TEC12705. This does mean the designed thermoelectric module has better cooling performance and hence, it is valid.

The rate of heat dissipation through the internal heat sinks has to be equal to or less than the cooling capacity of the TEC module. The rate of heat dissipation through external heat sinks has to be equal to or more than the heat rejected at the hot sides of the TEC module. These two cases are well satisfied in this thesis design.

The aerodynamic drag coefficient for the hatchback car ranges between 0.26 to 0.31. Toyota Vitz is categorized under hatchback car. According to the product information or specification (datasheets) of Toyota Yaris, the aerodynamic drag coefficient for the Toyota Yaris/Vitz 2005-2011 is 0.29. The drag coefficients obtained from CFD analysis in this thesis are 0.273 for the baseline car and 0.275 for the car with the cooling system. The deviation is about 6.2% for the baseline car and 5.4% for the car with the cooling system from the drag coefficient of the actual vehicle. The deviation is due to the shape variations between the model and the actual vehicle. It is less than 10%. So, it is acceptable.

Therefore, it can be concluded that the design results in this study are valid.

5.5. Demonstration of Thermoelectric Cooling System

The collected data from the temperature test for the demonstration is presented in Table 5.4 below.

As shown in Table 5.4 and Table 5.5, the cabin temperature of the car model increases at a faster rate for the first 20 minutes of parking time. Later, it decreases its rate but continues to rise gradually. For the car model with the thermoelectric cooling system switched off, the cabin temperature rises from 28.5 ℃ to 39.5 ℃ on the first trial, from 28 ℃ to 39.6 ℃ on the second trial and form 27.5 ℃ to 39.9 ℃ on the third trial within 44 minutes. On the other hand, the cabin air temperature of the model when the cooling system running rises from 27.5 ℃ to 36.4 ℃ on the first trial, from 28.5 ℃ 36.2 ℃ on the second trial and from 28 ℃ to 36.2 ℃ on the third trial within the same time interval. This indicates that the temperatures of the cabin air are lower for the model with the cooling system running than that of the model with no cooling system running. For the same time interval, they have a temperature difference of greater than 3 ℃ for all trials. The cabin air temperature for the model when no thermoelectric cooling system is running is found to be higher.

The average temperature of the cabin air of the three trials when the thermoelectric cooling system was not running is 2.3 ℃ higher than the temperature of cabin air when the cooling system running.

Table 5.4: Recorded temperatures for the demonstration for trials one & two

	Trial 1				Trial 2			
	Without cooler		With cooler		Without cooler		With cooler	
Time (min.)	T_{amb} (℃)	T_{cabin} (℃)	T_{amb} (℃)	T_{cabin} (℃)	T_{amb} (℃)	T_{cabin} (℃)	T_{amb} (℃)	T_{cabin} (℃)
0	28.50	28.50	27.50	27.50	28.00	28.00	28.50	28.50
4	29.10	32.10	28.40	31.50	28.20	31.50	29.60	31.90
8	28.60	34.00	29.50	34.40	28.30	33.40	29.70	33.00
12	29.50	35.80	29.80	35.40	28.50	34.90	30.20	35.20
16	28.00	37.00	29.20	36.00	28.00	35.80	29.60	35.00
20	28.60	37.40	29.50	36.40	28.40	36.60	29.60	35.40
24	29.00	37.80	30.20	36.30	29.10	37.00	30.00	36.00
28	28.70	38.40	29.90	36.20	28.90	37.30	30.00	36.40
32	28.80	39.00	29.50	36.30	29.20	37.80	30.10	36.30
36	27.90	39.00	29.70	36.10	29.40	38.70	30.60	36.40
40	28.40	38.80	29.40	36.50	29.10	39.40	30.50	36.30
44	28.20	39.60	29.50	36.40	28.80	39.60	30.60	36.20
Average	28.60	36.44	29.34	34.91	28.65	35.83	29.91	34.71

The difference of average ambient temperatures of the three trials between when the cooler was running and when the cooler was switched off is 0.6℃. This implies that the trial conducted when the cooling system was operating was with a higher ambient temperature than when not running. Therefore, it gives an additional point to the thermoelectric cooling system.

Generally, the thermoelectric cooling system demonstrated could reduce the temperature rise of cabin air by more than 2.3 ℃ degrees Celsius for 44 minutes. The result is low because a very coarse aluminum fin, which has a low heat dissipation rate, is used. The car body used to make the cabin model is made with aluminum sheet metal which, has high thermal conductivity. It conducts more thermal energy into the car cabin. The thermal grease (paste) which should have been used between the TEC and

Table 5.5: The recorded temperature for the demonstration on trial three

	Trial 3			
	Without cooler		With cooler	
Time (min.)	T_{amb} (℃)	T_{cabin} (℃)	T_{amb} (℃)	T_{cabin} (℃)
0	27.5	27.5	28	28
4	28.1	29.5	28.50	31.20
8	28.5	33.1	28.20	33.50
12	27.9	35.6	28.70	35.10
16	28.00	36.1	29.00	35.50
20	28.40	36.5	28.90	36.10
24	28.10	37	28.40	36.30
28	27.00	38.2	28.30	35.80
32	27.6	39	27.90	36.30
36	28.2	39.8	27.80	36.00
40	28.5	39.5	28.00	36.40
44	28.3	39.9	28.30	36.20
Average	28.30	35.97	28.20	34.70

the aluminum heat sinks are not used due to their unavailability. It is a thermal conductor and could increase the heat transfer from the cabin air to the TEC through the internal aluminum heat sink if could have been used.

CHAPTER SIX

CONCLUSIONS AND RECOMMENDATIONS

6.1. Summary

In this thesis work, an automatic thermoelectric cooling system is designed. The cooling load of the car cabin is analytically estimated. Some components of the thermoelectric cooling system have also been designed. The design includes the design of internal and external heat sinks, design of the TEC module. The design of heat sinks was based on the way that the dimensions of the heat sinks got fixed and the fin thickness was optimized. The heat dissipation rate versus the fin thickness was analyzed. The design of a TEC module with an optimum cooling power of 35.92 W at a temperature gradient of 24.865℃ is obtained. Selection of a compatible solar panel for the car cabin is made. To estimate the aerodynamics effects of the thermoelectric cooling system, two-car models of which one is with the cooling system assembled and another with no cooling system, are simulated in ANSYS 19.3 R3. Demonstration for the automatic thermoelectric cooling system is also made.

6.2. Conclusions

From this thesis, the following conclusions are drawn.

- ❖ The thermoelectric cooling system dissipates heat from the car cabin at a rate of 267.24 W. This is about 31.01% of the total heat gain by the vehicle cabin from different heat sources. This does mean it can reduce the rate of the temperature rise of a car cabin parked exposed to sunlight, by 31.01%.
- ❖ The aerodynamic drag at the car speed of 120 km/hr which is assembled with the cooling system is 0.273 while for the car which did not install the cooling system, is 0.275. The rise in the aerodynamic drag coefficient is 0.02. It is a 0.73% increase.
- ❖ The additional fuel consumption for the car at a speed of 120 km/hr due to the installation of the thermoelectric cooling system is 0.037 Li/hr.
- ❖ As the cooling system works on a solar panel installed on the roof of the car, the solar heat gain by the roof is minimized by the panel, which is here used as a solar shield.

6.3. Recommendations

To increase the optimum cooling capacity of the thermoelectric cooler:

- ❖ It is good to enhance the performance of the TEC module in some means. The research should go deeply into thermoelectricity to replace the existing A/C as thermoelectric cooling is environmentally-green.

6.4. Future Scope of Research

This topic can further be extended to the following areas.

- ❖ Experimental investigation of the thermoelectric cooling system can be conducted by preparing a prototype of a car.
- ❖ The position of external cooling fans may be relocated and used along with ducts to draw the hot air from the heat sinks. They could also be installed at different locations such as at the door panels.
- ❖ The topic might also be conducted in a truck cabin.
- ❖ The aerodynamic drag can be reduced by using a spoiler.

SPECIAL ACKNOWLEDGMENT

This research project is funded by Adama Science and Technology University under the grant number ASTU/SM-R/316/21, Adama, Ethiopia.

REFERENCES

Abdel-Fadeel, W. A., Abd-Fadeel, W. A., Soubhi, &, & Hassanein, A. (2014). Temperature variations, inside a parked car in hot and dry climates https://www.researchgate.net/publication/259577084

Abdul, A. P. J., & Uit, K. (2017). a Study & Analysis of Thermoelectric Refrigeration System With Environment. *International Research Journal of Engineering and Technology (IRJET)*, *4*(4), 259–264. https://www.irjet.net/archives/V4/i4/IRJET-V4I452.pdf

Abdulsalam, O., Santoso, B., & Aries, D. (2007). Cooling Load Calculation and Thermal Modeling for Vehicle by MATLAB. *International Journal of Innovative Research in Science, Engineering and Technology*, *3297*(5), 3052–3060. https://doi.org/10.15680/IJIRSET.2015.0405076

Agarwal, N., & Khan, E. (2008). Automobile Air Conditioning System. *International Research Journal of Engineering and Technology*. www.irjet.net

Barrubeeah, M., Rady, M., Attar, A., Albatati, F., & Abuhabaya, A. (2021). Design, modeling and parametric optimization of thermoelectric cooling systems for high power density electronic devices. *International Journal of Low-Carbon Technologies*, 1–17. https://doi.org/10.1093/ijlct/ctab032

Bjurling, F. (2013). Transient thermal model of a minibus' cabin and optimization of the air-conditioning control strategies. https://www.diva-portal.org/smash/get/diva2:667344/FULLTEXT01.pdf

Cooke, D. B. (2018). Design and Optimization of a Self-powered Thermoelectric Car Seat Cooler.

Equations, I. (n.d.). Chapter 3 Thermoelectric Coolers.

Fayazbakhsh, M. A., & Bahrami, M. (2013). Comprehensive modeling of vehicle air conditioning loads using heat balance method. *SAE Technical Papers*, *2*(x). https://doi.org/10.4271/2013-01-1507

FRANKLIN, E. D. (2018). an Investigation Into Thermoelectric Coolers. *The Lancet*, *268*(6946), 762–765.

Gillott, M., Jiang, L., & Riffat, S. (2010). An Investigation Of Thermoelectric Cooling Devices For Small-Scale Space Conditioning Applications In Buildings. *International Journal of Energy Research*, *34*(9), 776–786. https://doi.org/10.1002/er.1591

Goldsmid, H. J. (2016). Optimisation and selection of semiconductor thermoelements. In *Springer Series in Materials Science* (Vol. 121). https://doi.org/10.1007/978-3-662-49256-7_4

Hargreaves, G. H. (1978). Estimation of Solar Radiation. *Paper - American Society of Agricultural Engineers*, 1–19.

Hrushabh, M., Patil, C., Patil, O., & Mahale, T. (2019). *Design & Development of Thermoelectric Cooler Using Peltier Plate*. *6*(3), 2393–2395. https://doi.org/10.17148/IARJSET.2019.6304

Huang, B. J., Chin, C. J., & Duang, C. L. (2000). A design method of thermoelectric cooler Â lectrique Conception d ’ un refroidisseur thermoe. *International Journal of Refrigeration*, *23*, 208–218.

John, A., Thomas, J., Kattukaran, J. S., Baby, R., & Vazhappilly, C. V. (2014). Solar Powered Heat Control System for Cars. In *Int Journal of Engineering Research and Applications www.ijera.com* (Vol. 4, Issue 5). www.ijera.com

Lethwala, Y., & Garg, P. (2017). Development of Auxiliary Automobile Air Conditioning System by Solar Energy. *International Research Journal of Engineering and Technology*. www.irjet.net

Mani, P. I. (2016). Design , Modeling and Simulation of a Thermoelectric Cooling System (TEC). *Master’s Theses*.

Maragkos, G. (2021). Review of Convective Heat Transfer Modelling in CFD Simulations of Fire-Driven Flows.

Marshall, G. J., Mahony, C. P., Rhodes, M. J., Daniewicz, S. R., Tsolas, N., & Thompson, S. M. (2019). Thermal Management of Vehicle Cabins, External Surfaces, and Onboard Electronics: An Overview. *Engineering*, *5*(5), 954–969. https://doi.org/10.1016/j.eng.2019.02.009

Mohiuddin, A. K. M., Osman, A., & Uddin, M. F. (2019). Development and investigation of a cooling system for a parked vehicle using solar energy. *International Journal of Recent Technology and Engineering*, *7*(6), 87–92.

Nair, M., & Tripathi, B. (2019). Experimental Studies on Thermoelectric Refrigeration System.

Pache, G. S., Tamse, A. B., & Surkar, B. K. (2014). HVAC (Heat Ventilation and Air Conditioning System) Using TEC (Thermoelectric Couple). *2014*, 28–33.

Patil, A. M. (2014). Review of Thermoelectric Air To Air Cooling For Cars. *III*(Iv), 48–51. http://www.ijltemas.in/DigitalLibrary/Vol.3Issue4/48-51.pdf

Raut, M. S., Heat, M. T., & Engg, P. (2012). Thermoelectric Air Cooling For Cars. *International Journal of Engineering Science and Technology*, *4*(05), 2381–2395.

Sarbu, I., & Dorca, A. (2018). A comprehensive review of solar thermoelectric cooling systems. *International Journal of Energy Research*, *42*(2), 395–415. https://doi.org/10.1002/er.3795

Shams, S., Poon, K., Aljunaibi, A., Tariq, M., Salem, F., & Ruta, D. (2016). Solar powered air cooling for idle parked cars: Architecture and implementation. *Proceedings - 2015 11th International Conference on Innovations in Information Technology, IIT 2015, October 2017*, 239–243. https://doi.org/10.1109/INNOVATIONS.2015.7381547

Singh, P. (2015). Alternate System for Car Cabin Comfort Cooling-Solar Powered. In *International Journal of Mechanics and Thermodynamics* (Vol. 6, Issue 1). http://www.irphouse.com

Siouane, S., Jovanovic, S., & Poure, P. (2016). A Novel Identification Method of Thermal Resistances of Thermoelectric Modules Combining Electrical Characterization Under Constant Temperature and Heat Flow Conditions. *Transactions on Environment and Electrical Engineering*, *1*(4), 44. https://doi.org/10.22149/teee.v1i4.72

Sunawar, A., & Garniwa, I. (2017). Maximum potential of the car cabin temperature in the outdoor parking conditions as a source of energy in thermoelectric generator. *IOP Conference Series: Materials Science and Engineering*, *180*(1). https://doi.org/10.1088/1757-899X/180/1/012104

Tadele, D. (2020). Experimental Investigation of PCM Integrated Solar Dryer for Fish Drying By A Thesis Submitted to Department of Thermal and Aerospace Engineering School of Mechanical , Chemical and Materials Engineering Office of Graduate Studies Adama Science and Technology University.

Tadesse, M. (2015). Thermal Comfort for Passenger Train from Dire-Dawa to Djibouti. *Masters Thesis, Approved by Board of Examiners, AASTU.*

Tritt, T. M. (2002). Thermoelectric Materials: Principles, Structure, Properties, and Applications. *Encyclopedia of Materials: Science and Technology*, 1–11. https://doi.org/10.1016/b0-08-043152-6/01822-2

Vaghela, J. K., & Kapadia, R. G. (2014). The load calculation of automobile air conditioning system. *International Journal of Engineering Development and Research*, *2*(1), 97–109.

Vetrivel, R., & Mohhammed Shafee, S. (2015). Design and analysis of solar thermo electric refrigerator. *International Journal of Applied Engineering Research*, *10*(76), 365–370.

Vinofer, B. P. (2016). Cooling Load Calculation and Design.

Wiley, J. (2011). Heat Sinks , Thermoelectrics , Heat Pipes , Compact Heat Exchangers , and Solar Cells.

APPENDIX A

Table A.1: Thermo-physical properties of gases at atmospheric pressure

T (K)	ρ (kg/m^3)	c_p (kJ/kg · K)	$\mu \cdot 10^7$ (N · s/m^2)	$\nu \cdot 10^6$ (m^2/s)	$k \cdot 10^3$ (W/m · K)	$\alpha \cdot 10^6$ (m^2/s)	Pr
Air							
100	3.5562	1.032	71.1	2.00	9.34	2.54	0.786
150	2.3364	1.012	103.4	4.426	13.8	5.84	0.758
200	1.7458	1.007	132.5	7.590	18.1	10.3	0.737
250	1.3947	1.006	159.6	11.44	22.3	15.9	0.720
300	1.1614	1.007	184.6	15.89	26.3	22.5	0.707
350	0.9950	1.009	208.2	20.92	30.0	29.9	0.700
400	0.8711	1.014	230.1	26.41	33.8	38.3	0.690
450	0.7740	1.021	250.7	32.39	37.3	47.2	0.686
500	0.6964	1.030	270.1	38.79	40.7	56.7	0.684
550	0.6329	1.040	288.4	45.57	43.9	66.7	0.683
600	0.5804	1.051	305.8	52.69	46.9	76.9	0.685
650	0.5356	1.063	322.5	60.21	49.7	87.3	0.690
700	0.4975	1.075	338.8	68.10	52.4	98.0	0.695
750	0.4643	1.087	354.6	76.37	54.9	109	0.702
800	0.4354	1.099	369.8	84.93	57.3	120	0.709

APPENDIX B

Table B. 1: Properties of solid materials

		Properties at 300 K				Properties at various temperatures (K) k (W/m · K)/c_p (J/kg · K)									
Composition	Melting point (K)	ρ (kg/m^3)	c_p (J/kg · K)	k (W/m · K)	$\alpha \cdot 10^6$ (m^2/s)	100	200	400	600	800	1000	1200	1500	2000	2500
Aluminum															
Pure	933	2702	903	237	97.1	302	237	240	231	218					
						482	798	949	1033	1146					
Alloy 2024-T6 (4.5% Cu, 1.5% Mg, 0.6% Mn)	775	2770	875	177	73.0	65	163	186	186						
						473	787	925	1042						
Alloy 195, Cast (4.5% Cu)		2790	883	168	68.2			174	185						
								—	—						
Beryllium	1550	1850	1825	200	59.2	990	301	161	126	106	90.8	78.7			
						203	1114	2191	2604	2823	3018	3227	3519		
Bismuth	545	9780	122	7.86	6.59	16.5	9.69	7.04							
						112	120	127							
Boron	2573	2500	1107	27.0	9.76	190	55.5	16.8	10.6	9.60	9.85				
						128	600	1463	1892	2160	2338				
Cadmium	594	8650	231	96.8	48.4	203	99.3	94.7							
						198	222	242							
Chromium	2118	7160	449	93.7	29.1	159	111	90.9	80.7	71.3	65.4	61.9	57.2	49.4	
						192	384	484	542	581	616	682	779	937	
Cobalt	1769	8862	421	99.2	26.6	167	122	85.4	67.4	58.2	52.1	49.3	42.5		
						236	379	450	503	550	628	733	674		
Copper															
Pure	1358	8933	385	401	117	482	413	393	379	366	352	339			
						252	356	397	417	433	451	480			
Commercial bronze	1293	8800	420	52	14		42	52	59						

APPENDIX C

Table C.1: Recorded temperature of the test for a Toyota Vitz car, which is parked facing south on direct sunlight from 12:00 AM to 1:00 PM.

Time (min.)	Cabin air temperature (^{0}c)	Inside surface temperature (℃) (Dashboard)	Outside surface temperature			
			Roof	Front windshield glass	Rear windshield glass	Right Side glass
0	35	56	34.3	37.8	36	40.2
10	38.5	57	35	38.3	38.7	39
20	41.2	59	35.5	40.1	41.5	41.5
30	43.8	58	42.7	41.6	45.5	42.6
40	45.7	56	43	40	42.9	43.8
50	45.9	58	44.5	41.3	45	42.7
60	44.5	57	45	44.3	43.7	42.7